BIOENGINEERING

A bioadhesive pacing lead for atraumatic cardiac monitoring and stimulation in rodent and porcine models

Jue Deng[1]†, Jingjing Wu[1], Xiaoyu Chen[1], Tiffany L. Sarrafian[2], Claudia E. Varela[3], William Whyte[3], Chuan Fei Guo[4], Ellen T. Roche[1,3], Leigh G. Griffiths[5]*, Hyunwoo Yuk[1]*‡, Christoph S. Nabzdyk[6]*§, Xuanhe Zhao[1,7]*

Current clinically used electronic implants, including cardiac pacing leads for epicardial monitoring and stimulation of the heart, rely on surgical suturing or direct insertion of electrodes to the heart tissue. These approaches can cause tissue trauma during the implantation and retrieval of the pacing leads, with the potential for bleeding, tissue damage, and device failure. Here, we report a bioadhesive pacing lead that can directly interface with cardiac tissue through physical and covalent interactions to support minimally invasive adhesive implantation and gentle on-demand removal of the device with a detachment solution. We developed 3D-printable bioadhesive materials for customized fabrication of the device by graft-polymerizing polyacrylic acid on hydrophilic polyurethane and mixing with poly(3,4-ethylenedioxythiophene):poly(styrenesulfonate) (PEDOT:PSS) to obtain electrical conductivity. The bioadhesive construct exhibited mechanical properties similar to cardiac tissue and strong tissue adhesion, supporting stable electrical interfacing. Infusion of a detachment solution to cleave physical and covalent cross-links between the adhesive interface and the tissue allowed retrieval of the bioadhesive pacing leads in rat and porcine models without apparent tissue damage. Continuous and reliable cardiac monitoring and pacing of rodent and porcine hearts were demonstrated for 2 weeks with consistent capture threshold and sensing amplitude, in contrast to a commercially available alternative. Pacing and continuous telemetric monitoring were achieved in a porcine model. These findings may offer a promising platform for adhesive bioelectronic devices for cardiac monitoring and treatment.

INTRODUCTION

Implantable temporary epicardial pacing leads have been clinically adopted to protect patients from the risk of postoperative arrhythmias including complete heart blocks during the recovery period after cardiac surgery. These pacing leads usually remain in place and connect with external pacemaker for the potential needs of cardiac pacing for 1 to 2 weeks (*1*–*4*). The temporary pacing leads must then be removed, which is typically accomplished by pulling on the external portion of the leads (*2*, *3*, *5*). Electrophysiological sensing and stimulation of such pacing leads requires an intimate bioelectronic interface between the implant and the target organ (*6*–*10*). Existing bioelectronic implants are surgically fixed to the target tissue by suturing or directly inserting the electrodes into the tissue (*11*–*16*). The traumatic and invasive nature of existing approaches come with a risk of undesirable outcomes, such as bleeding, fluid accumulation around the heart, and heart tissue damage during implantation or removal of the devices in clinical practice (*17*, *18*). These complications can potentially compromise the reliability and electrophysiological function of the device. In particular, conventional methods can impose risk in crucial organs such as the heart with adverse outcomes (*1*, *19*), including device failure (*20*, *21*), heart chamber perforation (particularly on the atrium) (*18*), hemorrhage (*3*), pericardial effusion, and cardiac tamponade (*17*). Therefore, bioelectronic implants capable of directly interfacing with organs without surgical fixation or direct electrode insertion are highly desirable yet remain an unmet need in the field.

Tissue adhesives have recently been adopted as an alternative fixation method to facilitate the sutureless integration of implantable bioelectronic devices with tissues (*22*–*26*). Existing tissue adhesives are manufactured separately from bioelectronic devices and applied as an adjunct to the targeted devices or tissues during the implantation process (*25*–*27*). This two-step approach can substantially increase the complexity of the implantation process, especially when targeting dynamic and nonuniform tissues such as the heart. An additional adhesive application step can potentially lead to inconsistent integration and unreliable electrical interfacing. Furthermore, the ad hoc application of separately manufactured tissue adhesives may result in adhesion in undesired locations or residual materials upon removal of the device.

Here, we developed a bioadhesive pacing lead to address the limitations of existing devices and methods. The bioadhesive pacing lead is an all-in-one device that is implanted without sutures, tissue puncture, or glue because it directly adheres to cardiac tissue. It is designed for continuous cardiac monitoring and pacing and on-demand retrieval. We developed a multimaterial three-dimensional

[1]Department of Mechanical Engineering, Massachusetts Institute of Technology, Cambridge, MA, USA, 02139. [2]Department of Thoracic Surgery, Mayo Clinic, Rochester, MN 55905, USA. [3]Institute for Medical Engineering and Science, Massachusetts Institute of Technology, Cambridge, MA 02139, USA. [4]Department of Materials Science and Engineering, Southern University of Science and Technology, Shenzhen 518055, China. [5]Department of Cardiovascular Medicine, Mayo Clinic, Rochester, MN 55905, USA. [6]Department of Anesthesiology and Perioperative Medicine, Mayo Clinic, Rochester, MN 55905, USA. [7]Department of Civil and Environmental Engineering, Massachusetts Institute of Technology, Cambridge, MA 02139, USA.
*Corresponding author. Email: zhaox@mit.edu (X.Z.); hyunwooyuk@sanaheal.com (H.Y.); griffiths.leigh@mayo.edu (L.G.G.); cnabzdyk@mgb.org (C.S.N.)
†Present address: Academy for Engineering and Technology, Fudan University, Shanghai 200438, China.
‡Present address: SanaHeal Inc., Cambridge, MA 02139, USA.
§Present address: Department of Anesthesiology, Perioperative, and Pain Medicine, Brigham and Women's Hospital, Harvard Medical School, Boston, MA 02115, USA.

(3D)–printing method to print all the components, including the electrode, insulation, and bioadhesive, in an integrated manner. The bioadhesive pacing lead is compatible with existing clinical equipment and protocols for cardiac pacing (*2*, *3*). We found that the high charge injection capacity (CIC; more than 450 μC cm^{-2}) of the bioadhesive pacing lead provided stable electrophysiological performance with higher R wave amplitude for cardiac monitoring and lower capture threshold for cardiac pacing compared with commercially available epicardial pacing leads. The device was tested for a clinically relevant period of 2 weeks for temporary epicardial pacing in rat and porcine models in vivo. This bioadhesive pacing lead offers a promising platform not only for bioelectronic diagnosis and treatment of patients with cardiac diseases but also for the future development of next-generation implantable electronics.

RESULTS

Minimally invasive bioadhesive pacing lead was manufactured by multimaterial 3D printing

To meet the clinical scenario of temporary cardiac pacing (fig. S1A) and address the limitations of existing devices and methods (fig. S1, B and C), the bioadhesive pacing lead was designed with an adhesive interface for mechanical and electrical integration with epicardium and a built-in reservoir for delivery of an on-demand detachment solution to the pacing lead (Fig. 1A and fig. S2). An electrode wire and a fluidic catheter were connected to the bioadhesive interface and the reservoir, respectively. Minimally invasive implantation tools, including a thermoformed balloon catheter, a customized adapter, and a sheath catheter, were assembled on the top of the bioadhesive pacing lead (Fig. 1A). For implantation, the folded bioadhesive pacing lead was designed to be inserted through the sheath catheter for delivery to the epicardium (Fig. 1B). The bioadhesive interface was designed to adhere to the epicardial surface by absorbing the water on the tissue surface and forming cross-links with the extracellular matrix of the epicardium (fig. S3) (*22*, *24*). Inflation of the balloon catheter unfolds the pacing lead, and subsequently the adapter provides a gentle pressure to facilitate adhesion to underlying tissue (Fig. 1B). The electrode wire can be connected to an existing cardiac pacing system, allowing the device to be readily incorporated into existing clinical setups for bidirectional electrical communication for electrocardiogram (ECG) monitoring and continuous cardiac pacing (Fig. 1B). To remove the device, a biocompatible detachment solution can be injected into the built-in reservoir for cleavage of physical and chemical cross-links between the bioadhesive interface and the underlying epicardial tissue for atraumatic detachment (Fig. 1B).

We used a multimaterial 3D-printing method to print the electrode, insulation, and bioadhesive components of the device for flexible, customized, and streamlined fabrication (fig. S4 and movie S1). To generate the 3D-printable bioadhesive ink, a hydrophilic polyurethane was first graft polymerized with polyacrylic acid (fig. S5A). These are two widely used polymers in biomaterials and medical devices without allergic reactions (*28*–*33*). This polymer was then dissolved in 70% ethanol solution and mixed with 1-ethyl-3-(3-dimethylaminopropyl)carbodiimide (EDC) and *N*-hydroxysulfosuccinimide sodium salt (sulfo-NHS) to obtain the nonconductive 3D-printable bioadhesive ink (*22*, *24*). The polyurethane was graft polymerized with a monomer containing a disulfide bond to provide the on-demand detachment capability of the bioadhesive polymer ink (fig. S5B). The printed bioadhesive materials were proposed to interact with the tissue through carboxylic acid groups and primary amines for the formation of physical and covalent cross-links (fig. S3). The detachment solution was designed to disrupt these physical cross-links through sodium bicarbonate (fig. S6A) and to cleave disulfide bonds of the detachable polymer by reduced L-glutathione (fig. S6B). Unless specified otherwise, the detachable bioadhesive polymer ink was used in the study.

The conductive bioadhesive ink was prepared by mixing nonconductive bioadhesive ink with an aqueous solution of a conducting polymer of 5% (w/w) PEDOT:PSS. For both nonconductive and conductive bioadhesive inks, the apparent viscosity decreased as the shear rate increased, showing typical non-Newtonian fluid behavior (Fig. 1C). The shear storage modulus initially remained relatively constant as shear stress increased, indicating a solid-like response where the material can store elastic energy (Fig. 1D). These shear-thinning and shear-yielding properties allowed the fabrication of bioadhesive electronics by direct-ink-writing 3D printing (*34*, *35*). The conductive ink was printed first, followed by the nonconductive bioadhesive layer (Fig. 1E, fig. S4, and movie S1). After printing, the inks were converted into a bioadhesive interface by evaporating the solvents (ethanol and water) in the inks, and scanning electron microscopy (SEM) images showed homogeneous distributions of PEDOT:PSS and 3D-printable bioadhesive polymer (Fig. 1F and fig. S7, A and B). NMR spectroscopy showed representative peaks of PEDOT:PSS and printed bioadhesive polymer (fig. S7C). After connecting a lead wire to the bioadhesive interface, a built-in reservoir was manufactured by printing a polyvinyl alcohol (PVA) sacrificial layer and an electrically insulating polyurethane layer. A fluidic tube was connected, and then another PVA sacrificial layer was printed on the top of the insulating polyurethane for connecting a thermoformed balloon catheter before folding the device and assembling with customized adaptor and sheath catheter (Fig. 1, E and F). After the printing and evaporating process, both the nonconductive and conductive bioadhesives were bound to the polyurethane with similar adhesion strength, likely because of polymer chain entanglements (fig. S8).

The bioadhesive pacing lead showed tissue-like mechanical properties, tissue adhesion, and reliable electrical properties

The bioadhesive interface showed anisotropic swelling where swelling was greatest perpendicular to the adhesion interface, which may minimize the potential geometric mismatch in wet physiological environments (fig. S9). The fully swollen material had a Young's modulus of 90 ± 22 kPa for the nonconductive bioadhesive and 490 ± 35 kPa for the conductive bioadhesive (Fig. 2A), demonstrating properties similar to cardiac tissue, which has a Young's modulus of approximately 10 to 500 kPa (*36*, *37*). The adhesive materials showed stretchability (maximum stretched length/initial length > 1.8 ± 0.1 times) (Fig. 2A) and high toughness (fracture toughness of 156 ± 12 J m^{-2} for the nonconductive bioadhesive and 437 ± 39 J m^{-2} for the conductive bioadhesive) (fig. S10). Integration of the bioadhesive pacing lead did not cause mechanical alteration to the underlying cardiac tissue (Fig. 2B) and provided adhesion sufficient to lift 400 g of porcine heart ex vivo (Fig. 2C).

A biocompatible aqueous detachment solution of 50 mM sodium bicarbonate and 50 mM reduced L-glutathione in phosphate-buffered saline (PBS) was delivered through the fluidic tube to the

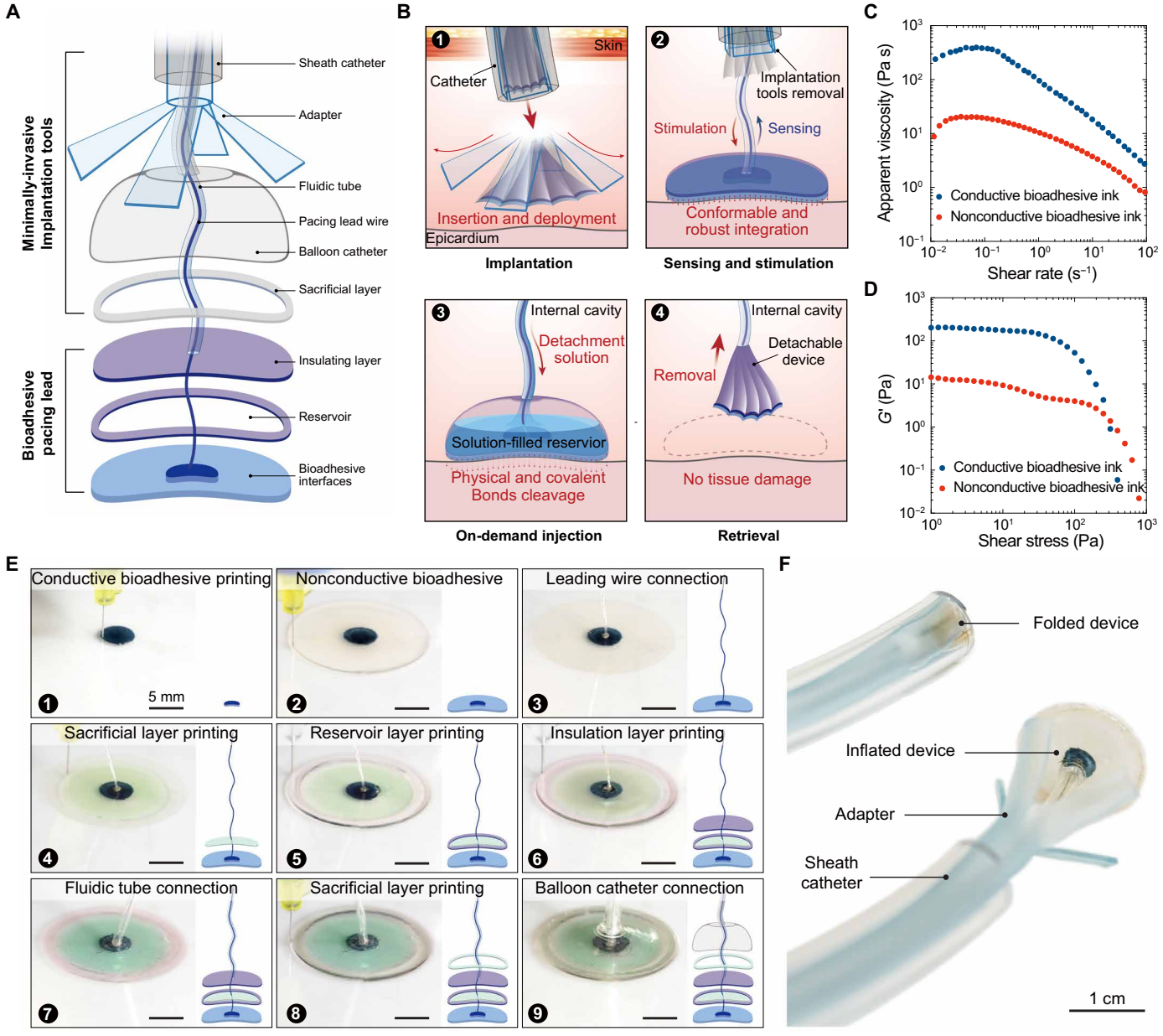

Fig. 1. Design and fabrication of the bioadhesive pacing lead. (**A**) Design of the bioadhesive pacing lead and minimally invasive implantation tools. (**B**) Schematic illustration of the adhesive implantation on the epicardium, sensing and stimulation, on-demand injection of detachment fluid to the built-in reservoir, and retrieval of the bioadhesive pacing lead. (**C**) Apparent viscosity as a function of shear rate for the nonconductive bioadhesive (red) and conductive bioadhesive inks (blue). $n = 3$ independent samples. (**D**) Shear storage modulus (G') as a function of shear stress for the nonconductive bioadhesive (red) and conductive bioadhesive (blue) inks. $n = 3$ independent samples. (**E**) Sequential images of 3D-printing process of the bioadhesive pacing lead. Different color dyes (green for sacrificial ink; red for insulation ink) are mixed with the transparent inks to improve visualization. The conductive bioadhesive ink appears as dark blue. Scale bars, 5 mm. (**F**) Representative images of the folded and inflated bioadhesive pacing lead with the minimally invasive implantation tools. Scale bar, 1 cm. Schematic illustrations were generated with Adobe Illustrator 2024.

built-in reservoir to trigger detachment (Fig. 2D) (*38*). To test diffusion of the solution through the bioadhesive interface, the interface was adhered to a gelatin hydrogel, and rhodamine B was added to the aqueous detachment solution for visualization. Within 5 min, the fluorescent signal migrated into the underlying substrate, which indicated successful diffusion through the bioadhesive interface (fig. S11). The detachment solution caused a substantial decrease in shear strength [1.6 ± 0.3 kPa, nonconductive; (Fig. 2E); 1.2 ± 0.3 kPa, conductive (Fig. 2F); lap-shear test, ASTM F2255] and interfacial toughness [11 ± 4 J m^{-2}, nonconductive (Fig. 2G); 6 ± 4 J m^{-2}, conductive (Fig. 2H); 180° peel test, ASTM F2256] compared with PBS treatment. When PBS was used instead of the detachment solution, the bioadhesive materials maintained high shear strength (49 ± 6 kPa, nonconductive, $P = 0.0003$; 36 ± 6 kPa, conductive, $P = 0.0052$) and interfacial toughness (309 ± 44 J m^{-2}, nonconductive, $P = 0.0002$; 220 ± 66 J m^{-2}, conductive, $P = 0.0049$)

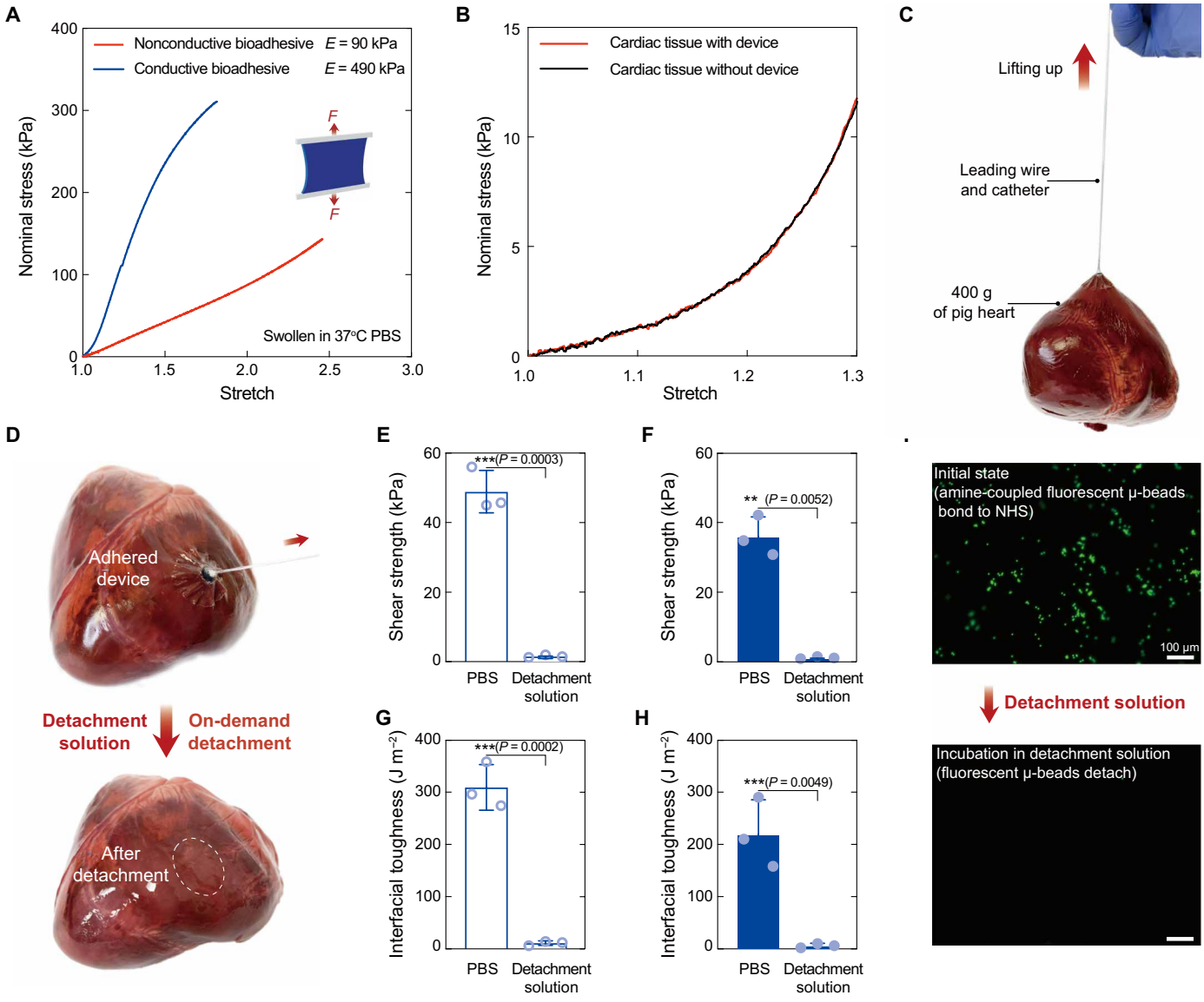

Fig. 2. The bioadhesive pacing lead has tissue-like mechanical properties and robust adhesive performance. (**A**) Nominal stress versus stretch curve of the nonconductive bioadhesive (red) or conductive bioadhesive (blue) fully swollen in PBS at 37°C. *E* is shown. *F* indicates tensile force applied to the sample. $n = 3$ independent samples. (**B**) Nominal stress versus stretch curve of ex vivo cardiac tissue with (red) and without (black) the adhered bioadhesive pacing lead. $n = 3$ independent samples. (**C**) Representative image of an ex vivo porcine heart (400 g) lifted by the adhered bioadhesive pacing lead. $n = 3$ independent samples. (**D**) Representative image of the bioadhesive pacing lead attached to a porcine heart (top) and the heart after detachment of the bioadhesive pacing lead (bottom). (**E** and **F**) Shear strength between ex vivo porcine heart tissues and polyurethane substrates adhered by (E) the nonconductive bioadhesive or (F) conductive bioadhesive, 5 min after applying PBS or the detachment solution. $n = 3$ independent samples per group. (**G** and **H**) Interfacial toughness between ex vivo porcine heart tissues and polyurethane substrates adhered by (G) the nonconductive bioadhesive or (H) conductive bioadhesive, 5 min after applying PBS or the detachment solution. $n = 3$ independent samples per group. (**I**) Representative fluorescent microscope images of fluorescent primary amine-coupled μbeads incubated on the bioadhesive interface in the initial state (top) and 10 min after incubation in the detachment solution. Scale, 100 μm. $n = 3$ independent samples. (E to H) Data are presented as mean ± SD. Statistical comparisons were evaluated by Student's *t* test, ** $P \leq 0.01$, *** $P \leq 0.001$.

(Fig. 2, E to H, and fig. S12). Amine-coupled fluorescent microbeads incubated on the bioadhesive were detached after incubation in detachment solution, further validating the cleavage of covalent bonds (Fig. 2I).

CIC and electrical impedance are two key parameters that are associated with cardiac pacing and monitoring performance in clinic applications (*4*). To measure the CIC of pacing leads, programmed stimulation waveforms (Fig. 3A) were administered by a pulse generator, and voltage-time curves (Fig. 3B) were acquired at increasing current amplitudes until the interface polarization reached the water electrolysis threshold. The CIC of the bioadhesive pacing lead reached 450 ± 25 μC cm^{-2}, which was higher than that of a commercially available temporary cardiac pacing lead (145 ± 23 μC cm^{-2}, $P < 0.0001$; Medtronic 6500) (Fig. 3, B and C). A cyclic CIC

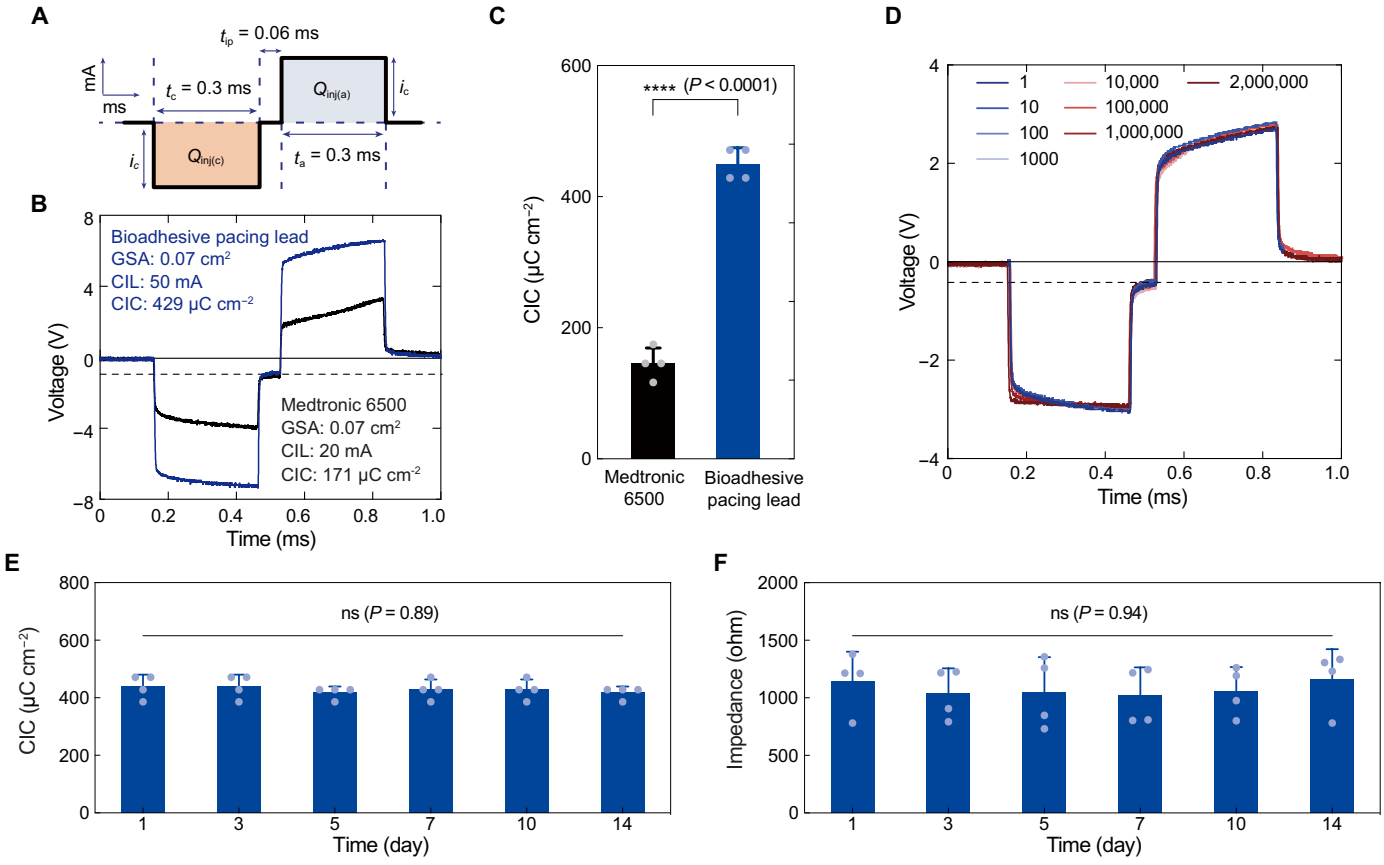

Fig. 3. The bioadhesive pacing lead demonstrated stable electrical properties. (**A**) Schematic diagram of a programmed stimulation waveform for CIC measurement. Current amplitude and pulse width of cathodic phase, 1_{ic} and t_c; current amplitude and pulse width of anodic phase, i_a and t_a; interphase delay duration, t_{ip}; injection charge of cathodic phase, $Q_{inj(c)}$; injection charge of anodic phase, $Q_{inj(a)}$. (**B**) Representative voltage transients acquired by the bioadhesive pacing lead (blue) or the Medtronic 6500 device (black) in PBS. GSA, geometric surface area; CIL, current injection limit. $n = 4$ independent samples. (**C**) CIC of the Medtronic 6500 and the bioadhesive pacing lead. $n = 4$ independent samples. (**D**) Voltage transients acquired by the bioadhesive pacing lead after 2 million charge-discharge cycles in PBS. Colored lines indicate cycle number. $n = 4$ independent samples. (**E**) CIC and (**F**) impedance at 1 kHz of the bioadhesive pacing lead in PBS over 14 days at 37°C. $n = 4$ independent samples. Data in (C), (E), and (F) are presented as means ± SD ($n = 4$ independent samples). Representative curves are presented in (B) and (D). Statistical significance was determined by the two-sided unpaired Student's *t* test between two groups (C) or one-way ANOVA and Tukey's multiple comparison test between more than two groups (E and F); ns, not significant; **** $P \leq 0.0001$.

measurement test showed that a stable CIC value was retained for more than 2 million charging and discharging cycles, supporting the electrochemical stability of the bioadhesive pacing lead (Fig. 3D). We further evaluated the stability of CIC (Fig. 3E), impedance (Fig. 3F), and conductivity (fig. S13) for 2 weeks of incubation in PBS at 37°C, which showed no significant difference in CIC ($P = 0.89$), impedance ($P = 0.94$), or conductivity ($P = 0.82$) during the incubation period.

The bioadhesive pacing lead supported reliable charge injection, atraumatic implantation, and retrieval in an ex vivo porcine heart

To visualize the pacing capability of the bioadhesive pacing lead compared with a commercial sutured pacing lead (Medtronic 4968), we applied the pacing leads on the surface of an ex vivo porcine heart that was periodically pressurized to simulate heartbeats (fig. S14 and movie S2). A light-emitting diode (LED) was placed near the bioadhesive pacing lead as an indicator of charge injection. The LED was illuminated directly in response to injection of electrical pulse to the porcine heart, indicating successful charge injection to the porcine heart (fig. S14A). We compared the threshold of the current pulse to activate the LED between the bioadhesive pacing lead and a commercially available epicardial pacing lead under the same experimental conditions. The bioadhesive pacing lead activated the LED at a lower electrical pulse (1.5 mA, 100 ms) than that delivered by commercial epicardial pacing lead (3.0 mA, 100 ms) (fig. S14, B and C). In addition, we demonstrated that the electrical pulse was effectively injected by the bioadhesive pacing lead at different frequencies (movie S2).

We demonstrated the minimally invasive implantation and retrieval of the bioadhesive pacing lead in an ex vivo porcine model (fig. S15 and movie S3). To simulate a minimally invasive surgical setting, a beating porcine heart was simulated using periodic pressured air inputs and a dark chamber with porcine abdomen tissue on the top. First, the bioadhesive pacing lead combined with an adapter and a balloon catheter was inserted through a sheath catheter to approach the epicardium (fig. S15, A and B). The balloon catheter was then inflated to unfold the bioadhesive pacing lead, and

the adapter was used to apply gentle pressure to form adhesion on the epicardium (fig. S15, C and D). Subsequently, saline was injected through the balloon catheter to dissolve the sacrificial layer of PVA between the balloon catheter and the attached pacing lead (fig. S15, E and F). For retrieval, we demonstrated that the detachment solution injected into the built-in reservoir removed the bioadhesive pacing lead without apparent tissue damage or remaining residues on the heart as examined by visual inspection (fig. S15, G and H).

The bioadhesive pacing lead exhibited cardiac monitoring and pacing based on in vivo rat models

For further evaluation in vivo, a rat model was tested by adhering the bioadhesive pacing lead to the ventricle of the rat heart with an electrode wire and a fluidic tube connected to a dorsal subcutaneous port (Fig. 4, A and B). For evaluation of continuous monitoring and pacing capability in vivo, the cathode and anode electrodes of an external pulse generator were connected to the bioadhesive pacing lead through the dorsal subcutaneous port and left foreleg, respectively (Fig. 4A). The heart was first exposed by a thoracotomy. Upon contact with the beating rat heart, the bioadhesive pacing lead adhered to the epicardium within 10 s under the application of gentle manual pressure (Fig. 4C). Adhesion was confirmed by gentle pulling of the lead. After the initial implantation, the bioadhesive interface provided mechanical integration and bidirectional electrical communication between the bioadhesive pacing lead and the rat cardiac tissue (movie S4). In contrast, a commercial temporary pacing lead (Medtronic 6500) required insertion into the myocardium for mechanical fixation and caused tissue bleeding (Fig. 4D and movie S5). As an additional control, nonadhesive polymer pacing leads were prepared by fully swelling the devices in PBS before implantation with suture or commercially available polymerizable tissue glue (BioGlue) (fig. S16). In contrast to the bioadhesive, tissue damage from suturing (fig. S16A) and undesirable spreading of unpolymerized glue (fig. S16B) decreased the reproducibility and effectiveness of the implantation process. These groups exhibited a fibrotic capsule around the lead-tissue interface (fig. S16C) or unstable fixation over time after 14 days (fig. S16D). We performed in vitro characterization of cytotoxicity and biocompatibility. Embryonic mouse fibroblasts cultured in medium preconditioned with the bioadhesive pacing lead showed comparable in vitro viability to those in Medtronic 6500–conditioned medium and control medium (unconditioned Dulbecco's minimal essential medium) after 24-hour cultures (fig. S17).

To evaluate continuous monitoring and pacing capability of the bioadhesive pacing lead in vivo, surface ECG signals were recorded simultaneously by subdermal needle electrodes. Capture threshold (the minimal electrical energy to effectively produce cardiac contraction) and the R wave amplitude of epicardial ECG were used to evaluate the stimulation and sensing capabilities of the bioadhesive pacing lead. The bioadhesive pacing lead successfully provided ventricular pacing of the rat heart as confirmed by the ventricular pacing spikes preceding each rhythm (QRS complex in ECG) and the increased heart rate from natural sinus rhythm [about 260 beats per minute (bpm)] to overdrive pacing rate (420 bpm) on day 0 (Fig. 4E and movie S4). We further confirmed successful ventricular pacing on day 7 (Fig. 4F) and day 14 (Fig. 4G) after implantation with the consistent ventricular-paced ECG rhythm suggesting stable integration of the bioadhesive lead. A commercially available temporary pacing lead (Medtronic 6500) also performed ventricular pacing at a higher capture pulse than the bioadhesive pacing lead (Fig. 4H), whereas it failed to capture on day 7 after implantation (Fig. 4, I and J). The average capture threshold of the bioadhesive pacing lead (1.3 mA, 0.5 ms) was significantly lower ($P = 0.01$) than that of the Medtronic 6500 (1.7 mA, 0.5 ms) on day 0 (Fig. 4J), consistent with the higher CIC of the bioadhesive pacing lead (Fig. 3C). The capture threshold of the bioadhesive pacing lead was stable during 14 days of implantation ($P = 0.19$) (Fig. 4J). In contrast, 25% of sutured (fig. S18, A to C) and 50% of BioGlue-fixed (fig. S18, D to F) pacing leads failed to capture on day 14 after implantation. Moreover, the remaining sutured or BioGlue-fixed pacing leads showed change in capture threshold between day 0 and day 14 (fig. S18G). The cardiac monitoring capability evaluated by average measured R wave amplitudes showed the that bioadhesive pacing lead did not change over 2 weeks in vivo ($P = 0.23$) (Fig. 4K). In contrast, the average R wave amplitudes were significantly decreased for BioGlue-fixed pacing lead ($P = 0.0004$) (fig. S18, H and I), sutured pacing lead ($P = 0.0132$) (fig. S18, H and J), and the Medtronic 6500 lead ($P < 0.0001$) (Fig. 4K and fig. S19).

To simulate the clinically relevant postoperative cardiac condition, we implemented a myocardial ischemia-reperfusion model in rat by left anterior descending coronary artery ligation and reperfusion (fig. S20, A to D) and evaluated the pacing capability of bioadhesive pacing leads before (fig. S20, E and F) and after ischemia-reperfusion injury (fig. S20, G to I). ECG waveform featuring ST-segment elevation substantiates the effective induction of myocardial ischemia (fig. S20, G and H). Bioadhesive pacing leads showed the ability to drive ventricular pacing of the rat heart after ischemia-reperfusion (fig. S20I), exhibiting a capture threshold comparable to that observed in a healthy rat heart.

For release of the bioadhesive pacing lead, the detachment solution was delivered through the fluidic channel from the dorsal port to the built-in reservoir of the device 14 days after implantation, allowing removal of the pacing lead (Fig. 4L). In contrast, removal of the Medtronic 6500 lead caused bleeding on the heart surface (Fig. 4M). Histological assessments by a blinded pathologist indicated that the bioadhesive pacing lead showed minimal to mild inflammatory response on day 14 after implantation to the rat heart (Fig. 4N). In contrast, the control groups of commercially available pacing leads (Medtronic 6500) (Fig. 4O) and sutured or BioGlue-fixed pacing leads (fig. S21) exhibited inflammation of the myocardial tissue. Immunofluorescence analysis showed that expression of CD3, CD68, collagen-I, and α–smooth muscle actin (α-SMA) for the bioadhesive pacing lead was significantly lower than those for Medtronic 6500 on day 14 after implantation ($P = 0.0029$, CD3; $P = 0.03$, CD68; $P = 0.0034$, collagen-I; $P = 0.004$, α-SMA) (fig. S22), which supported the histological evaluation. Moreover, the macroscopic (Fig. 4P) and histologic (Fig. 4Q) observations of the rat heart did not show evidence of residual implants or tissue trauma after on-demand retrieval of the bioadhesive pacing lead.

Complete blood counts and comprehensive blood chemistry panels showed results comparable to untreated rats without notable systemic toxicity after 2 weeks of implantation and 1 week after removal of the bioadhesive pacing leads (fig. S23). We further evaluated the systemic immune response by Luminex quantitative analysis of serum samples on day 14 after implantation for bioadhesive pacing lead and Medtronic 6500. The pro-inflammatory cytokines interleukin-6 (IL-6) and tumor necrosis factor–α showed lower expression for the bioadhesive pacing leads compared with

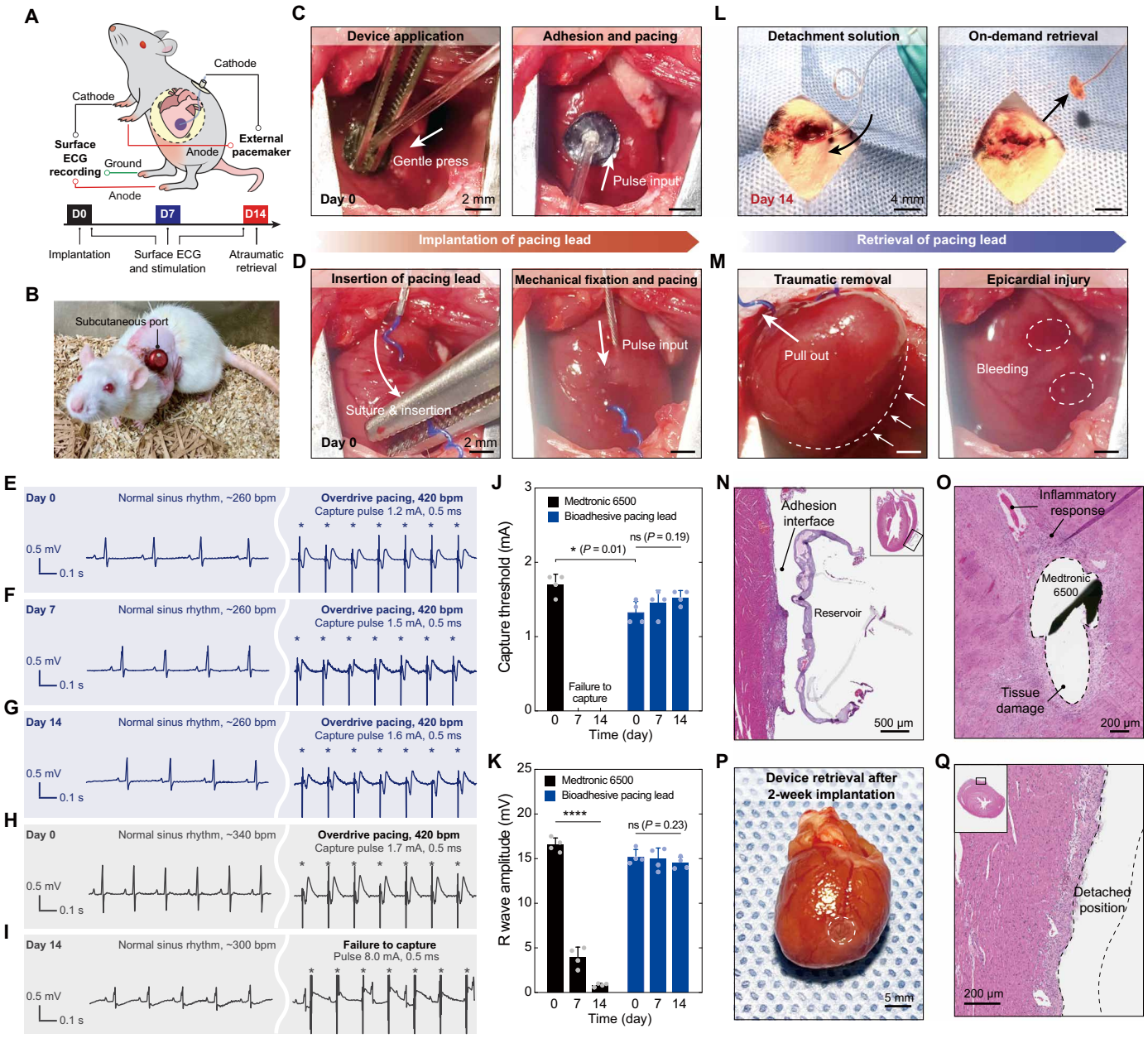

Fig. 4. The bioadhesive pacing lead allowed atraumatic implantation, retrieval, and stable cardiac monitoring and pacing in a rat model. (**A**) Schematic illustration of in vivo continuous epicardial pacing with surface ECG recording in rat model. D, day. (**B**) Representative image of a rat fitted with the subcutaneous port. (**C**) Representative image of the application and adhesion of the bioadhesive pacing lead on the rat heart. Scale bar, 2 mm. (**D**) Representative images of the insertion of a commercially available temporary pacing lead (Medtronic 6500) to the rat heart. Scale bar, 2 mm. (**E** to **G**) Representative ECG waveforms before (left) and after (right) ventricular pacing by the bioadhesive pacing lead on (E) day 0, (F) day 7, and (G) day 14 after implantations. (**H** and **I**) Representative ECG waveforms before (left) and after (right) ventricular pacing by the Medtronic 6500 temporary pacing lead on (H) day 0 and (I) day 14 after implantations. (**J**) Ventricular capture threshold on days 0, 7, and 14 after implantations. (**K**) R wave amplitude on days 0, 7, and 14 after implantations. (**L**) Representative images for atraumatic retrieval of the bioadhesive pacing lead from subcutaneous port on day 14 after implantation. Scale bar, 4 mm. (**M**) Representative images for retrieval of the commercial temporary pacing lead from the rat heart on day 0 after implantation. Scale bar, 2 mm. (**N** and **O**) Representative histology images stained with hematoxylin and eosin for (N) the bioadhesive pacing lead and (O) the Medtronic 6500 temporary pacing lead in rat hearts after 14 days after implantation. Scale bars, 500 μm (N) and 200 μm (O). (**P**) Representative gross image and (**Q**) histological image of a rat heart stained with hematoxylin and eosin after the retrieval of implanted bioadhesive pacing lead on day 14 after implantation. Scale bar, 5 mm (P) and 200 μm (Q). Values in (J) and (K) represent the means ± SD ($n = 4$ independent samples). (B to I) and (L to Q) showed representative curves and images ($n = 4$ independent samples per group). One-way ANOVA and Tukey's multiple comparison test. *$P < 0.05$. Schematic illustrations were generated with Adobe Illustrator 2024.

the Medtronic 6500. The bioadhesive pacing lead group showed higher serum concentrations of anti-inflammatory cytokine IL-13 compared with Medtronic 6500. All the other cytokines showed comparable values for both bioadhesive pacing lead and Medtronic 6500 implantation (fig. S24).

The bioadhesive pacing lead demonstrated atraumatic cardiac monitoring and pacing in porcine models in vivo

To further evaluate the proposed bioadhesive pacing lead in a large animal model, we demonstrated implantation, cardiac monitoring, single- and dual-chamber pacing, and retrieval of the bioadhesive pacing lead in a proof of concept in vivo porcine model, with a comparative analysis against a commercially available temporary pacing lead (Fig. 5A). After surgical exposure of the porcine heart, the bioadhesive pacing leads were adhered to the atrium and ventricle by application of gentle manual pressure for 10 s, and bleeding was not observed (Fig. 5B). Stable adhesion was maintained throughout the 2-week sensing and pacing studies (Fig. 5C), and the lead was successfully removed by injection of the detachment solution (Fig. 5D). After on-demand removal of the bioadhesive pacing lead, the underlying epicardial tissue did not show observable tissue damage, bleeding, or residual implant material, suggesting that this method did not cause tissue trauma (movie S6).

The commercially available temporary pacing lead was inserted into the ventricle (Fig. 5E) to accomplish mechanical fixation (Fig. 5F). This commercial temporary pacing lead showed myocardial damage and bleeding during both implantation and retrieval from the porcine heart (Fig. 5, E and G, and movie S7). Fixation of nonadhesive pacing lead was accomplished by positioning the lead on the heart and surgical suturing to the heart (fig. S25, A to C). During and after suturing the device to the heart, bleeding was observed (fig. S25, B to D), and histology confirmed tissue disruption at the suture point (fig. S25E). BioGlue was separately injected to the surface of the nonadhesive pacing lead to reinforce the physical contact (fig. S25, F to H). This implantation approach exhibited an undesirable spread of uncured glue to nearby tissues (fig. S25I) and the tissue-device interface (fig. S25J) because of movement and the nonflat surface of the heart.

The design of the bioadhesive pacing lead allowed compatibility with a clinical-grade pacing system (GE Mac-Lab hemodynamic recording system and Medtronic 5330 pulse generator) for bidirectional electrical communication, including R wave amplitude monitoring in real time (Fig. 5H) and continuous pacing of the porcine heart (Fig. 5, I to M, and movie S6). The electrical pulses generated by the external pulse generator were effectively delivered to the porcine heart for ventricular (Fig. 5I), atrial (Fig. 5J), and atrioventricular pacing (Fig. 5K) with high R wave amplitude (Fig. 5L) and low capture threshold (Fig. 5M). All paced rhythms were regular and stable, and we observed an increased heart rate from natural sinus rhythm (approximate 60 bpm) (Fig. 5H) to an overdrive pacing rate (110 to 120 bpm) (Fig. 5, I to K). To perform ventricular pacing, the lead was applied to the left ventricular free wall with successful ventricular pacing at a current pulse of 4 mA. A typical ventricular-paced rhythm with a wide QRS complex was observed, and the heart rate increased to 120 bpm, indicating successful ventricular capture. As a control, a commercial temporary pacing lead (Medtronic 6500) was inserted into the myocardial tissue at the same location on the left ventricular free wall to perform ventricular pacing (fig. S26 and movie S7). We compared the R wave amplitude and ventricular capture threshold, which are two key parameters to evaluate the sensing and pacing capability of cardiac pacing leads in clinical applications (*4*, *39*). The average R wave amplitude (9.4 mA) of the bioadhesive pacing lead was higher than that of the commercial pacing lead (4.7 mA) ($P = 0.05$) (Fig. 5L). In addition, the average capture threshold (4 mA) of the bioadhesive pacing lead was lower than that of the commercial pacing lead (7.3 mA) ($P = 0.05$) (Fig. 5M). For atrial pacing, the ECG waveform showed a typical narrow QRS complex and pacing spike before the non-sinus P wave and an increased heart rate (110 bpm), indicating successful atrial capture at 4 mA (Fig. 5J and movie S6). Furthermore, atrioventricular pacing was also successfully performed by two bioadhesive pacing leads adhered to the atrium and ventricle, validated by the characteristic sequentially paced rhythm with two spikes and wide QRS complex (Fig. 5K).

To continuously evaluate the performance of the bioadhesive pacing lead, the leads were connected to an implantable pacemaker and adhered to the ventricles in a survival porcine model (Fig. 6, A and B). The implantable pacemaker allowed for continuous monitoring of the capability of the bioadhesive pacing leads and was telemetrically detected and adjusted by an external portable programmer (Fig. 6C). The average R wave amplitudes of epicardial ECG, as measured by bioadhesive pacing lead on the ventricle, showed no significant difference on day 0 compared to day 10 after implantation ($P = 0.6584$) (Fig. 6D). Histology of the tissue showed the retained adhesion on the ventricular tissues and no inflammatory response on the tissue-device interface over 10 days (Fig. 6, E and F). Continuous ECG telemetry remained stable without abnormal events detected during the implantation period, and the epicardial ECG waveforms coincided with the surface ECG waveforms (Fig. 6G). In addition, the bioadhesive pacing leads enabled the performance of ventricular pacing with a low capture threshold of 4.2 V on day 10 after implantation. Clear pacing spikes and representative ECG waveforms during ventricular pacing were recorded in real time by the implantable pacemaker and portable programmer (Fig. 6H).

DISCUSSION

Implantation of temporary epicardial pacing leads is the standard of care for patients undergoing cardiac surgery (*1*, *3*, *40*). Temporary epicardial pacing helps to manage perioperative electrophysiological abnormalities, such as surgery-related high-degree heart blocks, that can result in severe bradycardia and hemodynamic collapse (*2*). Furthermore, optimal epicardial pacing can improve overall hemodynamics for both adult and pediatric patients in postcardiotomy (*41*, *42*). Whereas various pacing lead technologies have been in development (*43*), existing devices still rely on the traumatic screw-in or insertion fixation. Existing pacing devices and traumatic methods can cause undesirable and detrimental complications (*44*). At implantation, the need for surgical fixation of conventional devices puts patients at risk of hemorrhage, cardiac chamber perforation, and arrhythmia because of myocardial irritation associated with the device fixation. After implantation, inflammatory response and fibrosis can cause pacing-threshold elevation and potential loss of sensing or capture capability. During the removal of the pacing lead, the pulling on the external portion of the leads is associated with risks of hemorrhage, pericardial effusion, and tamponade (*45*–*47*). Furthermore, these risks are substantially increased for neonatal and pediatric patients considering the small size and thin walls of

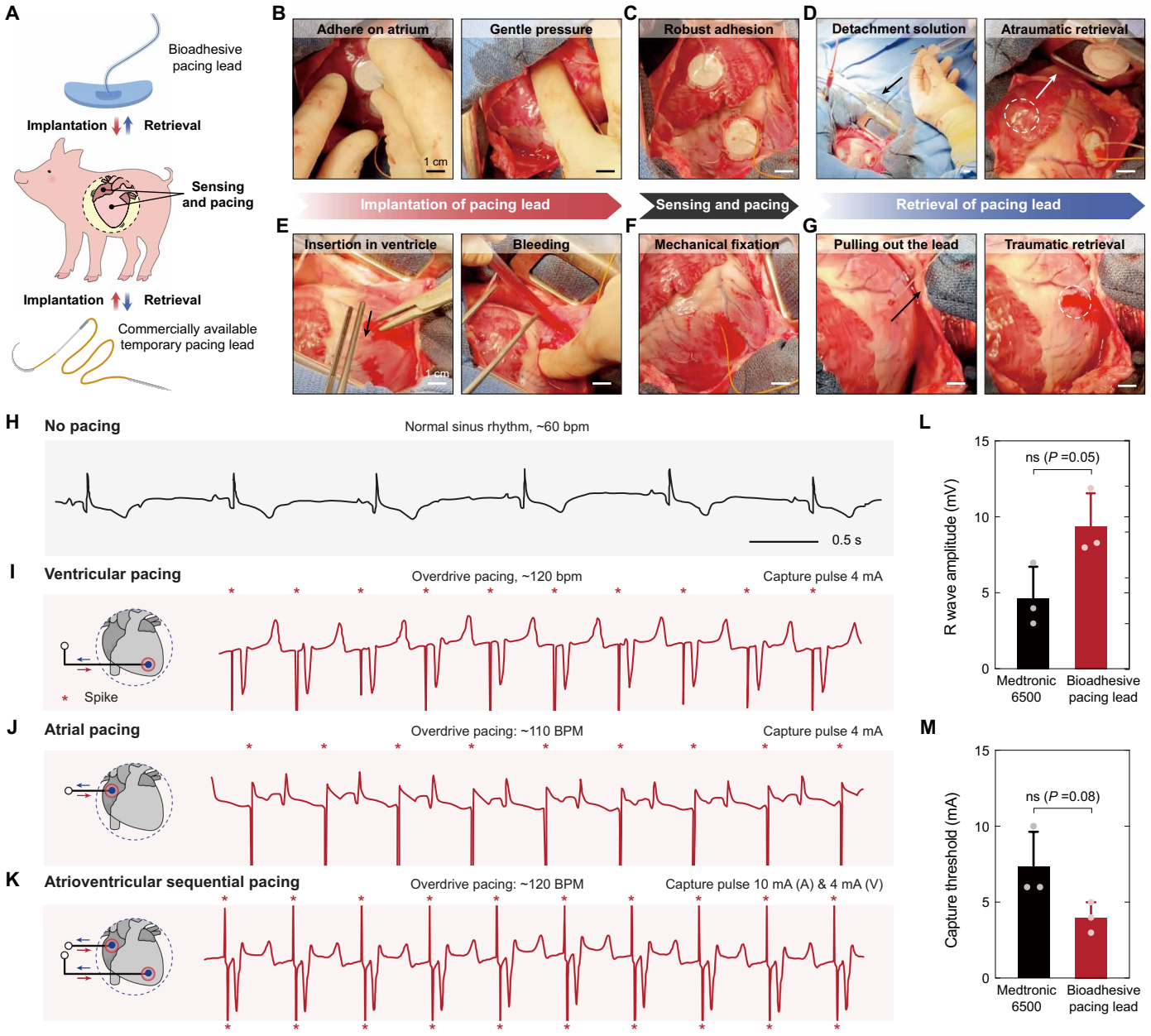

Fig. 5. The bioadhesive pacing lead allowed atraumatic implantation, retrieval, and effective cardiac monitoring and pacing in a porcine model. (**A**) Schematic illustration for in vivo cardiac pacing of porcine heart by the bioadhesive pacing lead and a commercially available temporary pacing lead (Medtronic 6500). (**B** to **D**) Representative images of (B) the placement, (C) continuous cardiac pacing, and (D) retrieval of the bioadhesive pacing lead. Scale bar, 1 cm. (**E** to **G**) Representative images of (E) the placement, (F) continuous cardiac pacing, and (G) retrieval of the commercially available temporary pacing lead. (**H**) Representative natural sinus rhythm with no pacing and a heart rate of 60 beats per minute (bpm). (**I**) Schematic illustration of lead placement on the ventricle and representative ventricular-paced ECG waveforms with an overdrive pacing rate of 120 bpm. The capture pulse of the bioadhesive pacing lead is 4 mA on the porcine ventricle. Asterisk (*) indicates a spike. (**J**) Schematic illustration of lead placement on the atrium and representative atrial-paced ECG waveform with an overdrive pacing rate of 110 bpm. The capture pulse of the bioadhesive pacing lead is 4 mA on the porcine atrium. (**K**) Schematic illustration and representative atrioventricular sequential paced ECG waveforms with an overdrive pacing rate of 120 bpm. The capture pulse is 10 mA on the porcine atrium and 4 mA on the porcine ventricle. (**L**) R wave amplitude sensed by the bioadhesive pacing lead and the commercial temporary pacing lead from the porcine heart. (**M**) Ventricular capture threshold of the bioadhesive pacing lead and the commercial temporary pacing lead. Values in (L) and (M) represent the means ± SD (bioadhesive pacing lead: $n = 3$ independent samples; Medtronic 6500: $n = 3$ independent measurements). Statistical comparisons were made by two-sided unpaired Student's t tests. Schematic illustrations were generated with Adobe Illustrator 2024.

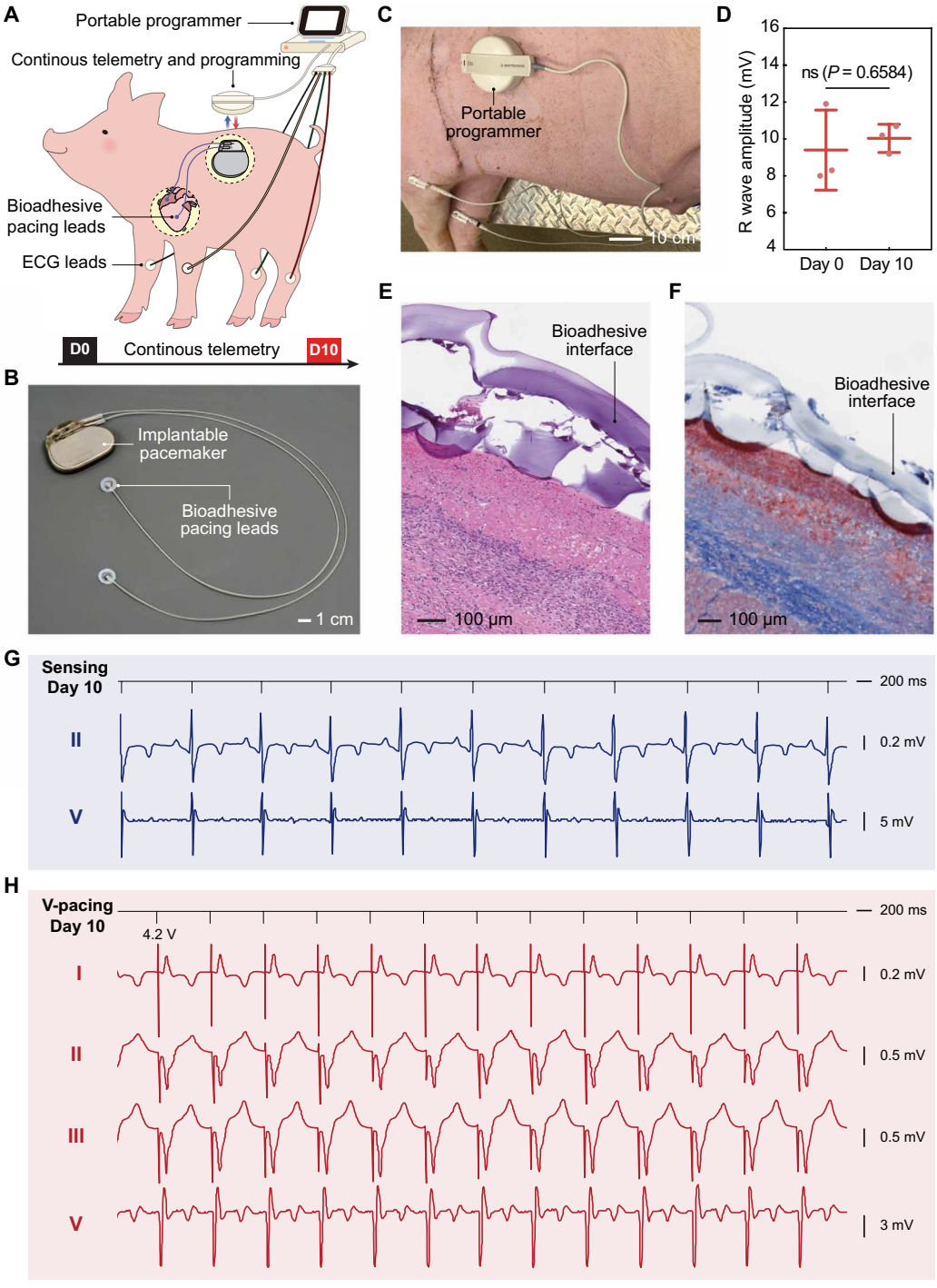

Fig. 6. Bioadhesive pacing lead supported continuous and telemetric cardiac monitoring and pacing in a porcine model. (**A**) Schematic illustration for continuous and telemetric cardiac monitoring and pacing by the bioadhesive pacing leads connected to an implantable pacemaker and adjusted by a portable programmer. (**B**) Representative image of the bioadhesive pacing leads connected to an implantable pacemaker by an international standard-1 (IS-1) connector. (**C**) Representative image of the telemetric monitoring and adjustment by a portable programmer. Scale bar, 1 cm. (**D**) R wave amplitudes on day 0 and day 10 after implantation. The R wave amplitudes were extracted from the epicardial ECG on ventricles and monitored telemetrically by a portable programmer. Scale bar, 10 cm. (**E** and **F**) Representative histology images stained with (E) hematoxylin and eosin and (F) Masson's trichrome for the bioadhesive pacing lead implanted to porcine heart on day 10 after implantation. Scale bars, 100 μm. (**G**) Representative surface ECG waveform recorded by subdermal electrodes (top) and epicardial ECG waveform (bottom) recorded by bioadhesive pacing lead on day 10 after implantation. (**H**) Representative ventricular-paced ECG waveforms on day 10 after implantation. The pulses (4.2 V, 0.4 ms) were delivered by the implantable pacemaker through the bioadhesive pacing leads and adjusted using the portable programmer. I, II, III, and V indicate the number of the electrodes. Values in (D) represent the means ± SD. $n = 3$ independent samples in (D) to (H). Statistical evaluation by two-sided unpaired t test. Schematic illustrations were generated with Adobe Illustrator 2024.

the heart and blood vessels (*21*, *48*). Hence, an epicardial pacing system that does not cause cardiac trauma yet provides stable and effective pacing capability has potential to improve safety and efficiency for patients.

In this study, we report a bioadhesive pacing lead for adhesive implantation, continuous cardiac monitoring and pacing, and on-demand retrieval in vivo. The current study aims to address the limitations of traumatic implantable bioelectronic devices and methods. A synergistic set of design, materials, and fabrication advances in bioadhesive electronics can overcome tissue-traumatic implantation and retrieval of devices, unreliable communication, and associated problems. Specifically, the 3D-printed bioadhesive interface provides mechanical integration and bidirectional electrical communications with the heart, offering flexibility in the fabrication of the device that is compatible with advanced manufacturing techniques such as multimaterial additive manufacturing. The bioadhesive interface provides stable ECG monitoring and a low capture threshold for cardiac pacing superior to commercially available cardiac pacing leads. The all-in-one electrofluidic design of the bioadhesive pacing lead provides continuous cardiac monitoring, pacing, and on-demand retrieval in a minimally invasive manner in vivo.

In addition, the bioadhesive pacing lead demonstrates various clinical advantages and possible benefits, which warrant further investigation to achieve clinical translation. The multimaterial 3D-printing–based fabrication allows the customization and personalization of cardiac devices including for adult and pediatric applications. The atraumatic characteristics of the bioadhesive pacing lead may offer a promising option for atrial pacing and synchronous atrioventricular pacing, which are technically challenging with existing devices because of the relatively thin wall of the atrium (*18*, *45*) and associated high risk of tissue trauma and massive hemorrhage (*1*). Furthermore, the bioadhesive pacing lead can readily be incorporated into the existing clinical settings and protocols for temporary cardiac pacing as demonstrated in the proof-of-concept in vivo porcine study, potentially benefiting future translation and adoption into clinics.

The current study also has several limitations and areas for future work. First, we demonstrated the efficacy of the bioadhesive pacing lead for up to 2 weeks after implantation, reflecting the typical clinical treatment regimens for temporary cardiac pacing (*3*). The long-term performance of the bioadhesive pacing lead, especially regarding the stability of adhesion and electrical performance for cardiac monitoring and pacing, will require further studies to investigate the feasibility and efficacy of the proposed platform for potential prolonged cardiac pacing applications. Second, long-term in vivo biocompatibility and tissue-implant interactions, such as fibrosis, beyond the time frame of temporary epicardial cardiac pacing (1 to 2 weeks) would require follow-up studies. Further improvements in materials and design of the bioadhesive pacing lead can also be explored to reduce the risk of fibrosis and pericardiac adhesion around the implanted lead for long-term applications (*49*). Third, the adoption of manufacturing technologies in the industry for scalable fabrication would further increase the mechanical robustness, electrical reliability, and reproducibility of bioadhesive pacing lead before clinical translation of the technology.

The bioadhesive pacing lead represents a paradigm for modulating electrophysiological activities of cardiac tissues in a minimally invasive manner. This strategy holds potential for extension into areas such as the peripheral nervous system, bladder, and spinal cord, paving the way for the development of a range of bioadhesive electronics. This study highlights its potential as a technology capable of effectively addressing the longstanding issues of invasiveness in tissue-electronics integration and associated unreliable functionalities.

MATERIALS AND METHODS

Study design

The aim of this study was to develop a bioadhesive pacing lead for atraumatic implantation, on-demand retrieval, and continuous cardiac monitoring and stimulation. We hypothesized that the bioadhesive pacing leads can address the limitations of the clinically adopted cardiac pacing leads while being readily compatible with the standard clinical setup. Mechanical characterization was performed to evaluate the adhesion to and detachment from the ex vivo porcine epicardial tissues. Structural and electrical characterizations were performed under physiological conditions to validate the structural and electrical stability. In vivo efficacy of continuous monitoring and stimulation was investigated in rat ($n = 4$ per group) and porcine ($n = 3$ per group) heart implantation models in comparison with a commercial epicardial pacing lead (Medtronic 6500), assessing the capture threshold and sensing amplitudes for 2 weeks. The atraumatic implantation and on-demand retrieval were assessed by animal monitoring, histopathological evaluation, immunofluorescence analysis, and blood analysis. For comparison, commercial epicardial pacing leads (Medtronic 6500 and 4968), nonadhesive pacing lead applied with a commercial glue (BioGlue) and surgical suturing were assessed following the same experimental conditions. The appropriate sample size for each study was chosen on the basis of similar evaluations in the literature. All tests were performed with randomly allocated experimental groups, and no data were excluded from the analyses. All animal study protocols and ethical compliance were reviewed and approved by the Institutional Animal Care and Use Committee at Massachusetts Institute of Technology (MIT) (for rat studies, protocol no. 1119-074-22) and at Mayo Clinic (for pig studies, protocol no. A00006340–21).

Materials

All chemicals (chemical pure grade) were obtained from Sigma-Aldrich unless otherwise mentioned and used without further purification. All porcine tissues and organs for ex vivo experiments were purchased from a research-grade porcine tissue vendor (Sierra Medical Inc.).

Preparation of 3D-printable bioadhesive ink

Hydrophilic polyurethane (PU) (HydroMed D3, AdvanSource Biomaterials) and 4,4′-methylenebis (phenyl isocyanate) were dried overnight in the vacuum condition before use. *N*,*N*-dimethylformamide (DMF) was distilled before use. PU (10 g) was dissolved in DMF (30 ml) for 2 hours at 50°C with a mechanical stirrer in a nitrogen environment to obtain a homogeneous mixture. Then, 2-hydroxyethyl methacrylate (0.6 ml) dissolved in 10 ml of DMF was added to the reaction mixture and stirred for 1 hour. To synthesize the nondetachable bioadhesive, azobis (isobutyronitrile) (AIBN; 0.3 ml) and acrylic acid (30 ml) were slowly added to the reaction mixture to prevent a sudden increase in viscosity. The reaction continued for 3 hours at 70°C. To synthesize detachable

bioadhesive and introduce disulfide bonds, 2-[[2-[(carboxymethyl) dithio]acetyl]oxy]ethyl 2-methyl-2-propenoate (3 g) and AIBN (0.3 ml) were added to the reaction mixture and stirred for 1 hour before adding acrylic acid monomer. The product was precipitated in distilled water to terminate the polymerization, and the product was cut into small pieces and thoroughly washed in distilled water to remove the remaining reactants. The final product was filtered and dried in the fume hood for 3 days to obtain nondetachable and detachable bioadhesive resin. The nondetachable and detachable bioadhesive resin was stirred and dissolved in 70% ethanol [15% (w/w)] to obtain nondetachable and detachable bioadhesive inks. To introduce NHS ester groups into the polyacrylic acid network, EDC [0.5% (w/w), Thermo Fisher Scientific] and sulfo-NHS [0.25% (w/w), Thermo Fisher Scientific] were mixed with the detachable bioadhesive ink and then mixed with nondetachable bioadhesive ink in a ratio of 1:1 (v/v) to obtain a 3D-printable bioadhesive ink.

To prepare 3D-printable electrically conductive bioadhesive ink, PEDOT:PSS pellets (Orgacon DRY5, AGFA) were dispersed in a deionized water–dimethyl sulfoxide mixture [water:dimethyl sulfoxide = 85:15 (v/v)] at a concentration of 5% (w/w), and the solution was mixed with the 3D-printable bioadhesive ink in a ratio of 1:2 (v/v) to obtain a 3D-printable conductive bioadhesive ink. The 3D-printable bioadhesive and conductive bioadhesive inks were filtered with 52-μm, 31-μm, and 18-μm nylon membrane filters (TISCH Scientific) consecutively before printing.

To prepare 3D-printable ink for the fabrication of the reservoir, hydrophilic polyurethane [25% (w/w); HydroThane, AdvanSource Biomaterials] was dissolved in a DMF-tetrahydrofuran (THF) mixture [DMF:THF = 50:50 (v/v)] at 70°C for 2 hours and then cooled down to room temperature to obtain an insulation ink. PVA [30% (w/w), weight-average molecular weight of 13,000 to 23,000) was dissolved in distilled water at 95°C for 2 hours and then cooled down to room temperature to obtain a PVA sacrificial ink.

Fabrication of bioadhesive pacing lead

3D printing of the bioadhesive pacing lead was conducted with a custom-designed 3D printer based on a Cartesian gantry system (AGS1000, Aerotech) with various sizes of nozzles (200- and 100-μm nozzles from Nordson EFD). Printing paths were generated by drawings (Adobe Illustrator) and converted into G-code by a commercial software package (CADFusion, Aerotech) to command the X-Y-Z motion of the printer head. The detailed printing paths are provided in fig. S4.

The bioadhesive interface was printed on a glass substrate, and an electrode lead wire (AS633, Cooner Wire) was connected to the printed bioadhesive interface by a silver paste (05002-AB, SPI Supplies). The PVA sacrificial layer was then printed on the dried bioadhesive interface. The insulation layer was printed on the top and connected with a PU-based fluidic channel (MRE25, Braintree Scientific Inc.) to obtain the bioadhesive pacing lead with a built-in reservoir. Nylon membrane filters (3 μm, TISCH Scientific) were added to replace the PVA sacrificial layer to physically separate the bottom adhesive and top insulation layers and to facilitate the detachment solution injection in the reservoir for terminal porcine studies.

To prepare a balloon catheter, a PU film was prepared by drop-casting PU solution [10% (w/w); HydroThane, AdvanSource Biomaterials] on the glass and evaporating the solvent. The PU film was thermally formed into a hemispherical balloon shape by a vacuum forming molding machine (JINTAI). The mold for the balloon was prepared by a stereolithography 3D printer (Form2, Formlabs). The balloon-shaped PU film was connected with a PU tube (MRE37, Braintree Scientific Inc.) and combined with the bioadhesive pacing lead by a printed ring-shaped sacrificial layer to serve as a balloon catheter. An adapter was prepared by thermal-forming a PU tube (McMaster Carr). The balloon catheter, adapter, and sheath catheter were assembled as an implantation tool for minimally invasive implantation of the bioadhesive pacing lead.

Mechanical characterization

To characterize the mechanical properties of the bioadhesive interface in the wet physiological condition, the nonconductive bioadhesive and conductive bioadhesive were equilibrated in 37°C PBS. The tensile properties and fracture toughness were measured using tensile tests of a rectangular sample (10 mm in length, 20 mm in width, and 0.2 mm in thickness) with a mechanical testing machine (20-N load cell, Zwick/Roell Z2.5). All tests were conducted with a constant tensile speed of 50 mm min^{-1}. Young's modulus (E) was obtained from the slope of the linear portion of the stress-strain curve. The fracture toughness was calculated on the basis of tensile tests of unnotched and notched samples (*50*).

For adhesion characterization, ex vivo porcine epicardial tissues and polyurethane substrates (HydroMed D3, AdvanSource Biomaterials) were adhered to the nonconductive bioadhesive or the conductive bioadhesive by pressing for 5 s (applying a pressure of approximate 1 kPa by either a mechanical test machine or an equivalent weight). All adhesion tests were performed 24 hours after applying the pressure to provide sufficient time for equilibrium swelling of the bioadhesive in wet environments. Poly(methyl methacrylate) films (50 μm thick, Goodfellow) were applied by using cyanoacrylate glue (Krazy Glue) as a stiff backing for the tissues and polyurethane substrates for the measurement of interfacial toughness and shear strength.

To measure the interfacial toughness, adhered samples (25 mm in width) were tested by the standard 180° peel test (ASTM F2256) with the mechanical testing machine (2.5-kN load cell, Zwick/Roell Z2.5). Interfacial toughness was calculated by dividing two times the plateau force by the width of the sample following the corresponding ASTM standard. To measure the shear strength, the adhered samples (25 mm in width and 10 mm in length) were tested by the standard lap-shear test (ASTM F2255) with the mechanical testing machine (2.5-kN load cell, Zwick/Roell Z2.5). Shear strength was determined by dividing the maximum force by the adhesion area of the sample following the corresponding ASTM standard. All tests were conducted with a constant tensile speed of 50 mm min^{-1}.

Rheological characterization

The bioadhesive and conductive bioadhesive inks were characterized by using a rotational rheometer (AR-G2, TA Instruments) with a 40-mm diameter and parallel-plate geometry. Apparent viscosity was measured as a function shear rate by steady-state flow tests with a logarithmic sweep of shear rate (0.01 to 100 s^{-1}). Shear storage modulus (G') was measured as a function of shear stress by oscillation test with a logarithmic sweep of shear stress (1 to 1000 Pa) at a frequency of 1 Hz. All rheological characterizations were conducted at 25°C with a preliminary equilibration time of 30 s.

Electrical characterization

To measure the CIC, the bioadhesive pacing lead and a platinum counter electrode were connected to a potentiostat (Autolab PGSTAT204, Metrohm). The bioadhesive pacing lead and an Ag/AgCl reference electrode were connected to an oscilloscope (Siglent Technologies). The potentiostat provided biphasic current inputs where a cathode phase of charge given by a certain amplitude and constant width (i_c, t_c) was followed by an interphase delay before symmetrical charge-balancing anodic phase with the same amplitude and width (i_a, t_a) (Fig. 4A). The current amplitude (i_c, i_a) was increased until the interface polarization (E_p) on the oscilloscope reached the electrochemical safety limit (cathodic water electrolysis, −0.8 V). The CIC was calculated by Eq. 1, and the charge injection capacity of commercial temporary myocardial pacing lead (Medtronic 6500) was measured on the basis of the same method (*51*).

$$Charge\ injection\ capacity = \frac{|i_c \times t_c| + |i_a \times t_a|}{Geometric\ surface\ area} \quad (1)$$

To measure the electrical impedance, the bioadhesive pacing lead was adhered on a gold-coated polyester film (McMaster Carr) and equilibrated in PBS before tests. The sensing and working electrodes of the potentiostat were connected to the lead wire of the bioadhesive pacing lead, and the counter and reference electrodes were connected to the gold-coated polyester film, respectively. The impedance and phase angle were measured in a range from 1 to 100,000 Hz in frequency. The conductivity of conductive bioadhesive was measured on the basis of the previously reported method (*24*). The length, width, and thickness of the sample were measured with a vernier caliper or a microscope (LV10, Nikon). To measure the electrical stability, samples were stored in PBS with 0.01% (w/v) sodium azide to prevent the growth of microorganisms during the test. The impedance of the bioadhesive pacing lead for the pig study with a 200-μm-thick adhesive layer was 680 ohms, which was measured by a Biotronik pacemaker and programmer.

Characterization of on-demand detachment

The detachment solution was prepared by dissolving 0.05 M sodium bicarbonate and 0.05 mM L-glutathione reduced in PBS. To validate the cleavage of chemical cross-links by the detachment solution, the bioadhesive interface was incubated in PBS with primary amine-coupled fluorescent microbeads (FluoSpheres; Thermo Fisher Scientific) for 30 min at room temperature. The samples were further incubated in the detachment solution for 5 min. The surface of the sample was characterized by a fluorescence microscope (LV; Nikon) after thorough washing with PBS to remove the noncrosslinked microbeads.

To characterize the diffusion of detachment solution through the bioadhesive interface to the underlying tissues, the bioadhesive pacing lead adhered on a gelatin hydrogel, and the detachment solution with a fluorescent dye (rhodamine B) was injected into the bioadhesive pacing lead for 1, 3, and 5 min, respectively. The detachment solution was fully removed before further characterization. The cross section of the sample was imaged by a laser confocal microscope (SP8, Leica). To prepare the gelatin hydrogel, 10% (w/w) gelatin powder was dissolved in deionized water at 37°C, followed by cooling down to room temperature for gelation.

Minimally invasive implantation and retrieval in ex vivo porcine model

All ex vivo experiments were reviewed and approved by the Committee on Animal Care at the Massachusetts Institute of Technology (protocol no. E18-06-0521). To simulate a minimally invasive surgical setting, the experiment was conducted inside a dark chamber with porcine abdomen tissue on the top. Periodic pressured air inputs (200 kPa, 150-ms duration, and 650-ms intermission) were introduced to the porcine heart to simulate heartbeats by a programmable pressure dispenser (Ultimus V, Nordson EFD). Two full-thickness holes in the porcine abdominal wall were created by a biopsy punch (10 mm, Integra), and two trocars (15 mm, Medtronic) were used to place an endoscope camera (DESPTECH) for visualization and the bioadhesive pacing lead through each trocar. The sheath catheter with a folded device was inserted through the trocar. A pressure-controlled syringe (Mercury Medical, AnapnoGuard Cuffill) was used to inflate the balloon catheter and open the bioadhesive pacing lead. An adapter was used to provide gentle pressure and form adhesion on the epicardium. Saline was injected through the balloon catheter to dissolve the PVA sacrificial layer, followed by robust adhesion of the bioadhesive pacing lead to the epicardium and retrieval of the balloon catheter. To achieve on-demand retrieval of the adhered bioadhesive pacing lead, the detachment solution was injected into the reservoir. After 5 min, the bioadhesive pacing lead was detached from the epicardium and retrieved through the trocar.

Simulated cardiac pacing in ex vivo porcine model

One LED was used as an indicator to quantitatively evaluate the efficacy of charge injection through pacing leads by comparing the current threshold to light up the LED. One electrode of the LED was inserted into the epicardium of an ex vivo porcine heart, and another electrode was connected to a potentiostat (Autolab PGSTAT204, Metrohm). The bioadhesive pacing lead or a commercially available sutured pacing lead (Medtronic 4968) was placed on the epicardium and connected to the potentiostat. The distance between the LED and the pacing leads remained consistent (2 cm) for both the bioadhesive pacing lead and the commercial pacing lead to ensure the same conductive pathway. The current pulse at different amplitudes and frequencies were provided by the potentiostat to evaluate the current threshold to light up the LED. Periodic pressured air inputs were introduced to the porcine heart to simulate heartbeats by the programmable pressure regulator (Ultimus V, Nordson EFD).

In vivo rat model

All studies in rats were approved by the MIT Committee on Animal Care (protocol no. 1119-074-22), and all surgical procedures and postoperative care were supervised by the MIT Division of Comparative Medicine (DCM) veterinary staff. Female Sprague Dawley rats (250 to 300 g, Charles River Laboratories) were used for all in vivo studies.

Before implantation, the bioadhesive pacing lead was prepared using aseptic techniques and was further sterilized for 1 hour under UV light. For continuous ventricular pacing, the rats were anesthetized using isoflurane (1 to 3% isoflurane in oxygen) in an anesthetizing chamber. Back hair and chest hair were removed. Endotracheal intubation was performed, and the rats were connected to a mechanical ventilator (Model 683, Harvard Apparatus) and placed over a heating pad for the duration of the surgery. For

measurement of surface ECG, anodic and cathodic subdermal needle electrodes were inserted into the skin of the left hind leg and right foreleg of a rat, respectively. A subdermal needle electrode was inserted into the skin of the right hind leg as a shared ground for surface ECG recording and epicardial pacing. The ECG signals were collected with data acquisition hardware (PowerLab and BioAmp, AD Instrument) and software (LabChart Pro 7, AD Instrument) for the duration of the surgery. The heart was exposed by a thoracotomy, and the pericardium was removed using fine forceps. A subdermal needle electrode was inserted into the skin of the left foreleg as an anodic pacing electrode. A bioadhesive pacing lead was adhered on the left ventricle ($n = 4$) as a cathodic pacing electrode. The lead wire and fluidic tube of the bioadhesive pacing lead were then tunneled subcutaneously from a ventral exit site close to the left fourth intercostal space to the dorsal side. The dorsal end of the lead wire and fluidic tube was inserted through a subcutaneous port. The subcutaneous port was placed by interrupted sutures (4-0 Vicryl, Ethicon) between the shoulder blades of the rat and covered by a protective aluminum cap (VABRC, Instech Laboratories) (*52*). An external stimulator (FE180, AD Instrument) was connected with the anodic and cathodic pacing electrodes and controlled by the data acquisition hardware and software (AD Instrument). Unipolar rectangular current pulses (0.5 ms, 0 to 3 mA, 5 to 7 Hz) were applied by the stimulator with continuous ECG recording to evaluate the capture threshold. The cardiac signals were sensed by the implanted pacing leads and recorded by the data acquisition hardware and software to evaluate the R wave amplitude. The incision was closed using interrupted sutures (4-0 Vicryl, Ethicon), and 3 to 6 ml of saline was administered subcutaneously. The animal was ventilated with 100% oxygen until autonomous breathing was regained, and the intubation catheter was removed.

On day 7 after implantation, each animal was anesthetized and connected to the data acquisition hardware (AD Instrument) for surface ECG recordings according to the procedure described above. Anesthesia was maintained using a nose cone, and the rats were placed over a heating pad for the duration of tests. The external stimulator was connected through the dorsal subcutaneous port. The continuous ventricle pacing and the capture threshold were examined by the surface ECG recordings. The animal was ventilated with 100% oxygen until autonomous breathing was regained.

On day 14 after implantation, the continuous ventricle pacing and capture threshold evaluation was conducted according to the procedure described above. For atraumatic retrieval, the dorsal subcutaneous port was removed first, and the detachment solution was injected from the dorsal end of the fluidic tube to the built-in reservoir. Five minutes after applying the detachment solution, the bioadhesive pacing leads were gently pulled out from the incision at the dorsal side. The animals were euthanized by CO_2 inhalation, and the hearts were excised and fixed in 10% formalin for 24 hours for histological analyses.

For evaluation of in vivo biocompatibility, the bioadhesive pacing leads ($n = 4$) and commercially available temporary pacing leads (Medtronic 6500; $n = 4$) were used. The bioadhesive pacing lead was applied to the heart according to the procedure described above. For the commercial pacing lead, the tip of the lead was inserted into the myocardium by a tapered point curved needle and fixed by a monofilament coil on the ventricle. The incision was closed using interrupted sutures (4-0 Vicryl, Ethicon), and 3 to 6 ml of saline was administered subcutaneously. The animal was ventilated with 100% oxygen until autonomous breathing was regained, and the intubation catheter was removed. At day 14 after implantation, the animals were euthanized by CO_2 inhalation and the hearts with the implants were excised and fixed in 10% formalin for 24 hours for histological analyses. All rats in the study were monitored daily by the MIT DCM veterinary staff and maintained normal health conditions. All fixed tissue samples were placed in 70% ethanol and submitted for histological processing and hematoxylin and eosin staining at the Hope Babette Tang (1983) Histology Facility at MIT.

In vivo porcine model

All studies in pigs were approved by the Mayo Clinic Institutional Animal Care and Use Committee at Rochester (protocol no. A00006340-21). Three female domestic pigs (100 to 110 kg, Manthei Hog Farm) were used for acute in vivo porcine studies ($n = 3$), and three pigs were used for survival porcine studies ($n = 3$). All animals were acclimatized in the holding facilities for 7 days before the study. Anesthesia was induced with tiletamine and zolazepam HCl (Telazol, 5 mg/kg, Zoetis), xylazine (2 mg/kg, Akorn animal house), and atropine (0.04 mg/kg intramuscularly, West-Ward) and maintained with isoflurane (1 to 3%, Baxter) in oxygen. Continuous ECG tracings, arterial blood pressure, and peripheral capillary oxygen saturation (SpO_2) percentage were monitored during the surgery (GE Mac-Lab hemodynamic recording system). Animals were intubated and placed on mechanical ventilation using volume-cycled ventilation. A left lateral thoracotomy was used to access the chest, and the pericardium was incised to expose the epicardium for device implantation. A commercially available pacing lead (Medtronic 6500) was inserted into the myocardium by a tapered point curved needle and fixed on the left ventricular free wall. The bioadhesive pacing lead was applied and adhered to the epicardium in the same region. Ventricular pacing was performed by the commercial pacing lead ($n = 3$) and the bioadhesive pacing lead ($n = 3$), respectively. Then, the bioadhesive pacing lead was applied and adhered to the right atrium. Atrial pacing and atrioventricular pacing were performed by the bioadhesive pacing leads. A dual chamber pulse generator (Medtronic 5330) was connected with pacing leads to perform all types of epicardial pacing to alter the heart rate (70 to 120 bpm). The pulse current was gradually increased to measure the capture threshold. The R wave amplitude of the commercial pacing lead and the bioadhesive pacing lead were recorded as the highest sensitivity setting for which intrinsic R waves were appropriately recognized on the pulse generator. After pacing, leads were removed either by manual traction (commercial leads) or instillation of the lead detachment solution through the fluidic port (bioadhesive pacing leads). At the end of the trial (maximum length was 4 hours), the animal was euthanized by an intravenous injection of sodium pentobarbitol (Fatal-Plus, 150 mg/kg, Baxter).

For the survival porcine study ($n = 3$ per group), bioadhesive pacing leads were applied and adhered to the ventricular free wall. The bioadhesive pacing leads modified with Oscor C/IS adaptors were tunneled and connected to an implantable pacemaker (Dextronix, PetPacer-DR), which was buried subcutaneously. The chests were surgically closed, and a RENAMIC portable implant programmer and interrogator were used to measure the sensing amplitude and pacing capture threshold telemetrically. On day 10 after implantation, the animal was euthanized, and the lead-cardiac tissue interface was collected for detailed histological evaluation.

Statistical analysis

Prism GraphPad (version 8) was used to assess the statistical significance of all comparison studies in this work. Data distribution was assumed to be normal for all parametric tests, but this was not formally tested. In the statistical analysis for comparison between multiple samples, one-way analysis of variance (ANOVA) followed by Tukey's multiple comparison test was conducted with thresholds of $P < 0.05$ considered significant. For the statistical analysis between two data groups, an unpaired two-sided Student's t test was used, and the significance threshold was set as $P < 0.05$. Significance level is presented throughout the figures as $^{*}P \leq 0.05$, $^{**}P \leq 0.01$, $^{***}P \leq 0.001$, and $^{****}P \leq 0.0001$.

Supplementary Materials

This PDF file includes:

Materials and Methods
Figs. S1 to S26

Other Supplementary Material for this manuscript includes the following:

Movies S1 to S7
Data file S1
MDAR Reproducibility Checklist

REFERENCES AND NOTES

1. P. del Nido, B. S. Goldman, Temporary epicardial pacing after open heart surgery: Complications and prevention. *J. Card. Surg.* **4**, 99–103 (1989).
2. M. D. Gammage, Temporary cardiac pacing. *Heart* **83**, 715–720 (2000).
3. A. S. Batra, S. Balaji, Post operative temporary epicardial pacing: When, how and why? *Ann. Pediatr. Cardiol.* **1**, 120–125 (2008).
4. S. S. Barold, R. X. Stroobandt, A. F. Sinnaeve, *Cardiac Pacemakers Step by Step: An Illustrated Guide* (John Wiley & Sons, 2008).
5. J. L. Austin, L. K. Preis, R. S. Crampton, G. A. Beller, R. P. Martin, Analysis of pacemaker malfunction and complications of temporary pacing in the coronary care unit. *Am. J. Card.* **49**, 301–306 (1982).
6. R. Feiner, T. Dvir, Tissue–electronics interfaces: From implantable devices to engineered tissues. *Nat. Rev. Mater.* **3**, 17076 (2018).
7. H. Yuk, B. Lu, X. Zhao, Hydrogel bioelectronics. *Chem. Soc. Rev.* **48**, 1642–1667 (2019).
8. L. Xu, S. R. Gutbrod, A. P. Bonifas, Y. Su, M. S. Sulkin, N. Lu, H.-J. Chung, K.-I. Jang, Z. Liu, M. Ying, C. Lu, R. C. Webb, J.-S. Kim, J. I. Laughner, H. Cheng, Y. Liu, A. Ameen, J.-W. Jeong, G.-T. Kim, Y. Huang, I. R. Efimov, J. A. Rogers, 3D multifunctional integumentary membranes for spatiotemporal cardiac measurements and stimulation across the entire epicardium. *Nat. Commun.* **5**, 3329 (2014).
9. J. Park, S. Choi, A. H. Janardhan, S.-Y. Lee, S. Raut, J. Soares, K. Shin, S. Yang, C. Lee, K.-W. Kang, H. R. Cho, S. J. Kim, P. Seo, W. Hyun, S. Jung, H.-J. Lee, N. Lee, S. H. Choi, M. Sacks, N. Lu, M. E. Josephson, T. Hyeon, D.-H. Kim, H. J. Hwang, Electromechanical cardioplasty using a wrapped elasto-conductive epicardial mesh. *Sci. Transl. Med.* **8**, 344ra386 (2016).
10. M. Kaltenbrunner, T. Sekitani, J. Reeder, T. Yokota, K. Kuribara, T. Tokuhara, M. Drack, R. Schwödiauer, I. Graz, S. Bauer-Gogonea, S. Bauer, T. Someya, An ultra-lightweight design for imperceptible plastic electronics. *Nature* **499**, 458–463 (2013).
11. I. R. Minev, P. Musienko, A. Hirsch, Q. Barraud, N. Wenger, E. M. Moraud, J. Gandar, M. Capogrosso, T. Milekovic, L. Asboth, R. F. Torres, N. Vachicouras, Q. Liu, N. Pavlova, S. Duis, A. Larmagnac, J. Vörös, S. Micera, Z. Suo, G. Courtine, S. P. Lacour, Electronic dura mater for long-term multimodal neural interfaces. *Science* **347**, 159–163 (2015).
12. E. T. Roche, M. A. Horvath, I. Wamala, A. Alazmani, S.-E. Song, W. Whyte, Z. Machaidze, C. J. Payne, J. C. Weaver, G. Fishbein, J. Kuebler, N. V. Vasilyev, D. J. Mooney, F. A. Pigula, C. J. Walsh, Soft robotic sleeve supports heart function. *Sci. Transl. Med.* **9**, eaaf3925 (2017).
13. Y. S. Choi, R. T. Yin, A. Pfenniger, J. Koo, R. Avila, K. B. Lee, S. W. Chen, G. Lee, G. Li, Y. Qiao, A. Murillo-Berlioz, A. Kiss, S. Han, S. M. Lee, C. Li, Z. Xie, Y.-Y. Chen, A. Burrell, B. Geist, H. Jeong, J. Kim, H.-J. Yoon, A. Banks, S.-K. Kang, Z. J. Zhang, C. R. Haney, A. V. Sahakian, D. Johnson, T. Efimova, Y. Huang, G. D. Trachiotis, B. P. Knight, R. K. Arora, I. R. Efimov, J. A. Rogers, Fully implantable and bioresorbable cardiac pacemakers without leads or batteries. *Nat. Biotechnol.* **39**, 1228–1238 (2021).
14. S. Huang, D. Lei, Q. Yang, Y. Yang, C. Jiang, H. Shi, B. Qian, Q. Long, W. Chen, Y. Chen, L. Zhu, W. Yang, L. Wang, W. Hai, Q. Zhao, Z. You, X. Ye, A perfusable, multifunctional epicardial device improves cardiac function and tissue repair. *Nat. Med.* **27**, 480–490 (2021).
15. J. Tang, J. Wang, K. Huang, Y. Ye, T. Su, L. Qiao, M. T. Hensley, T. G. Caranasos, J. Zhang, Z. Gu, K. Cheng, Cardiac cell–integrated microneedle patch for treating myocardial infarction. *Sci. Adv.* **4**, eaat9365 (2018).
16. Y. S. Choi, H. Jeong, R. T. Yin, R. Avila, A. Pfenniger, J. Yoo, J. Y. Lee, A. Tzavelis, Y. J. Lee, S. W. Chen, H. S. Knight, S. Kim, H.-Y. Ahn, G. Wickerson, A. Vázquez-Guardado, E. Higbee-Dempsey, B. A. Russo, M. A. Napolitano, T. J. Holleran, L. A. Razzak, A. N. Miniovich, G. Lee, B. Geist, B. Kim, S. Han, J. A. Brennan, K. Aras, S. S. Kwak, J. Kim, E. A. Waters, X. Yang, A. Burrell, K. S. Chun, C. Liu, C. Wu, A. Y. Rwei, A. N. Spann, A. Banks, D. Johnson, Z. J. Zhang, C. R. Haney, S. H. Jin, A. V. Sahakian, Y. Huang, G. D. Trachiotis, B. P. Knight, R. K. Arora, I. R. Efimov, J. A. Rogers, A transient, closed-loop network of wireless, body-integrated devices for autonomous electrotherapy. *Science* **376**, 1006–1012 (2022).
17. C. L. Cote, A. Baghaffar, P. Tremblay, C. Herman, Incidence of tamponade following temporary epicardial pacing wire removal. *J. Card. Surg.* **35**, 1247–1252 (2020).
18. V. Geyfman, R. H. Storm, S. C. Lico, J. W. Oren IV, Cardiac tamponade as complication of active-fixation atrial lead perforations: Proposed mechanism and management algorithm. *Pacing Clin. Electrophysiol.* **30**, 498–501 (2007).
19. E. Cingolani, J. I. Goldhaber, E. Marbán, Next-generation pacemakers: From small devices to biological pacemakers. *Nat. Rev. Cardiol.* **15**, 139–150 (2018).
20. B. Freedman, G. Boriani, T. V. Glotzer, J. S. Healey, P. Kirchhof, T. S. Potpara, Management of atrial high-rate episodes detected by cardiac implanted electronic devices. *Nat. Rev. Cardiol.* **14**, 701–714 (2017).
21. E. B. Fortescue, C. I. Berul, F. Cecchin, E. P. Walsh, J. K. Triedman, M. E. Alexander, Patient, procedural, and hardware factors associated with pacemaker lead failures in pediatrics and congenital heart disease. *Heart Rhythm* **1**, 150–159 (2004).
22. H. Yuk, C. E. Varela, C. S. Nabzdyk, X. Mao, R. F. Padera, E. T. Roche, X. Zhao, Dry double-sided tape for adhesion of wet tissues and devices. *Nature* **575**, 169–174 (2019).
23. J. Li, A. Celiz, J. Yang, Q. Yang, I. Wamala, W. Whyte, B. Seo, N. Vasilyev, J. Vlassak, Z. Suo, D. J. Mooney, Tough adhesives for diverse wet surfaces. *Science* **357**, 378–381 (2017).
24. J. Deng, H. Yuk, J. Wu, C. E. Varela, X. Chen, E. T. Roche, C. F. Guo, X. Zhao, Electrical bioadhesive interface for bioelectronics. *Nat. Mater.* **20**, 229–236 (2021).
25. Q. Yang, T. Wei, R. T. Yin, M. Wu, Y. Xu, J. Koo, Y. S. Choi, Z. Xie, S. W. Chen, I. Kandela, S. Yao, Y. Deng, R. Avila, T.-L. Liu, W. Bai, Y. Yang, M. Han, Q. Zhang, C. R. Haney, K. B. Lee, K. Aras, T. Wang, M.-H. Seo, H. Luan, S. M. Lee, A. Brikha, N. Ghoreishi-Haack, L. Tran, I. Stepien, F. Aird, E. A. Waters, X. Yu, A. Banks, G. D. Trachiotis, J. M. Torkelson, Y. Huang, Y. Kozorovitskiy, I. R. Efimov, J. A. Rogers, Photocurable bioresorbable adhesives as functional interfaces between flexible bioelectronic devices and soft biological tissues. *Nat. Mater.* **20**, 1559–1570 (2021).
26. K. Yamagishi, I. Kirino, I. Takahashi, H. Amano, S. Takeoka, Y. Morimoto, T. Fujie, Tissue-adhesive wirelessly powered optoelectronic device for metronomic photodynamic cancer therapy. *Nat. Biomed. Eng.* **3**, 27–36 (2019).
27. Y. Hong, F. Zhou, Y. Hua, X. Zhang, C. Ni, D. Pan, Y. Zhang, D. Jiang, L. Yang, Q. Lin, Y. Zou, D. Yu, D. E. Arnot, X. Zou, L. Zhu, S. Zhang, H. Ouyang, A strongly adhesive hemostatic hydrogel for the repair of arterial and heart bleeds. *Nat. Commun.* **10**, 2060 (2019).
28. K. Zheng, Q. Gu, D. Zhou, M. Zhou, L. Zhang, Recent progress in surgical adhesives for biomedical applications. *Smart Mater. Med.* **3**, 41–65 (2022).
29. L. Zhang, J. Liang, C. Jiang, Z. Liu, L. Sun, S. Chen, H. Xuan, D. Lei, Q. Guan, X. Ye, Z. You, Peptidoglycan-inspired autonomous ultrafast self-healing bio-friendly elastomers for bio-integrated electronics. *Natl. Sci. Rev.* **8**, nwaa154 (2021).
30. L. Zeng, J. He, Y. Cao, J. Wang, Z. Qiao, X. Jiang, L. Hou, J. Zhang, Tissue-adhesive and highly mechanical double-network hydrogel for cryopreservation and sustained release of anti-cancer drugs. *Smart Mater. Med.* **2**, 229–236 (2021).
31. C. Jiang, L. Zhang, Q. Yang, S. Huang, H. Shi, Q. Long, B. Qian, Z. Liu, Q. Guan, M. Liu, R. Yang, Q. Zhao, Z. You, X. Ye, Self-healing polyurethane-elastomer with mechanical tunability for multiple biomedical applications in vivo. *Nat. Commun.* **12**, 4395 (2021).
32. S. Chen, L. Sun, X. Zhou, Y. Guo, J. Song, S. Qian, Z. Liu, Q. Guan, E. M. Jeffries, W. Liu, Y. Wang, C. He, Z. You, Mechanically and biologically skin-like elastomers for bio-integrated electronics. *Nat. Commun.* **11**, 1107 (2020).
33. L. Zhang, Z. Liu, X. Wu, Q. Guan, S. Chen, L. Sun, Y. Guo, S. Wang, J. Song, E. M. Jeffries, C. He, F.-L. Qing, X. Bao, Z. You, A highly efficient self-healing elastomer with unprecedented mechanical properties. *Adv. Mater.* **31**, e1901402 (2019).
34. H. Yuk, B. Lu, S. Lin, K. Qu, J. Xu, J. Luo, X. Zhao, 3D printing of conducting polymers. *Nat. Commun.* **11**, 1604 (2020).
35. M. A. Skylar-Scott, J. Mueller, C. W. Visser, J. A. Lewis, Voxelated soft matter via multimaterial multinozzle 3D printing. *Nature* **575**, 330–335 (2019).
36. H. Jawad, N. N. Ali, A. R. Lyon, Q. Z. Chen, S. E. Harding, A. R. Boccaccini, Myocardial tissue engineering: A review. *J. Tissue Eng. Regen. Med.* **1**, 327–342 (2007).
37. M. Krishani, W. Y. Shin, H. Suhaimi, N. S. Sambudi, Development of scaffolds from bio-based natural materials for tissue regeneration applications: A review. *Gels* **9**, 100 (2023).
38. X. Chen, H. Yuk, J. Wu, C. S. Nabzdyk, X. Zhao, Instant tough bioadhesive with triggerable benign detachment. *Proc. Natl. Acad. Sci. U.S.A.* **117**, 15497–15503 (2020).

39. A. Sinnaeve, R. Willems, J. Bagkers, G. Holovoet, R. Stroobandt, Pacing and sensing: How can one electrode fulfill both requirements? *Pacing Clin. Electrophysiol.* **10**, 546–554 (1987).
40. P. Zoll, R. Zoll, R. Falk, J. Clinton, D. Eitel, E. Antman, External noninvasive temporary cardiac pacing: Clinical trials. *Circulation* **71**, 937–944 (1985).
41. H. R. Singh, A. S. Batra, S. Balaji, Pacing in children. *Ann. Pediatr. Cardiol.* **6**, 46–51 (2013).
42. M. I. Cohen, D. M. Bush, V. L. Vetter, R. E. Tanel, T. S. Wieand, J. W. Gaynor, L. A. Rhodes, Permanent epicardial pacing in pediatric patients: Seventeen years of experience and 1200 outpatient visits. *Circulation* **103**, 2585–2590 (2001).
43. G. C. Beaufort-Krol, H. Mulder, D. Nagelkerke, T. W. Waterbolk, M. T. E. Bink-Boelkens, Comparison of longevity, pacing, and sensing characteristics of steroid-eluting epicardial versus conventional endocardial pacing leads in children. *J. Thorac. Cardiovasc. Surg.* **117**, 523–528 (1999).
44. D. Luria, D. Bar-Lev, O. Gurevitz, H. Granit, Z. Rotstein, M. Eldar, M. Glikson, Long-term performance of screw-in atrial pacing leads: A randomized comparison of J-shaped and straight leads. *Pacing Clin. Electrophysiol.* **28**, 898–902 (2005).
45. J. A. Smith, J. Tatoulis, Right atrial perforation by a temporary epicardial pacing wire. *Ann. Thorac. Surg.* **50**, 141–142 (1990).
46. S. K. Mulpuru, M. Madhavan, C. J. McLeod, Y.-M. Cha, P. A. Friedman, Cardiac pacemakers: Function, troubleshooting, and management: Part 1 of a 2-part series. *J. Am. Coll. Cardiol.* **69**, 189–210 (2017).
47. P. K. Mishra, E. Lengyel, S. Lakshmanan, H. Luckraz, Temporary epicardial pacing wire removal: Is it an innocuous procedure? *Interact. Cardiovasc. Thorac. Surg.* **11**, 854–855 (2010).
48. K. C. Lau, J. W. Gaynor, S. M. Fuller, K. A. Smoots, M. J. Shah, Long-term atrial and ventricular epicardial pacemaker lead survival after cardiac operations in pediatric patients with congenital heart disease. *Heart Rhythm* **12**, 566–573 (2015).
49. L. M. Stapleton, A. N. Steele, H. Wang, H. L. Hernandez, A. C. Yu, M. J. Paulsen, A. A. A. Smith, G. A. Roth, A. D. Thakore, H. J. Lucian, K. P. Totherow, S. W. Baker, Y. Tada, J. M. Farry, A. Eskandari, C. E. Hironaka, K. J. Jaatinen, K. M. Williams, H. Bergamasco, C. Marschel, B. Chadwick, F. Grady, M. Ma, E. A. Appel, Y. J. Woo, Use of a supramolecular polymeric hydrogel as an effective post-operative pericardial adhesion barrier. *Nat. Biomed. Eng.* **3**, 611–620 (2019).
50. J.-Y. Sun, X. Zhao, W. R. Illeperuma, O. Chaudhuri, K. H. Oh, D. J. Mooney, J. J. Vlassak, Z. Suo, Highly stretchable and tough hydrogels. *Nature* **489**, 133–136 (2012).
51. G. Schiavone, X. Kang, F. Fallegger, J. Gandar, G. Courtine, S. P. Lacour, Guidelines to study and develop soft electrode systems for neural stimulation. *Neuron* **108**, 238–258 (2020).
52. W. Whyte, E. T. Roche, C. E. Varela, K. Mendez, S. Islam, H. O'Neill, F. Weafer, R. N. Shirazi, J. C. Weaver, N. V. Vasilyev, P. E. M. Hugh, B. Murphy, G. P. Duffy, C. J. Walsh, D. J. Mooney, Sustained release of targeted cardiac therapy with a replenishable implanted epicardial reservoir. *Nat. Biomed. Eng.* **2**, 416–428 (2018).

Acknowledgments: We thank the Koch Institute Swanson Biotechnology Center for technical support, specifically the Hope Babette Tang (1983) Histology Core for the histological processing and the Peterson (1957) Nanotechnology Materials Core for the resin embedding; R. Bronson at Harvard Medical School for the histological analyses; X. Yan for SEM imaging; and K. Mendez and B. Lu for insightful discussions. **Funding:** This work is supported by the National Institutes of Health (grant nos. 1R01HL153857-01 to X.Z. and 1R01HL167947-01 to L.G.G., C.S.N., and X.Z.), the National Science Foundation (grant no. EFMA-1935291 to E.T.R. and X.Z.), and the Department of Defense Congressionally Directed Medical Research Programs (grant no. PR200524P1 to X.Z.). **Author contributions:** J.D., H.Y., C.S.N., and X.Z. conceived the idea. J.D., H.Y., and X.Z. developed the bioadhesive pacing lead. X.C. and J.D. developed and synthesized the printable bioadhesive materials. J.D. conducted the mechanical and electrical characterizations. J.D. and H.Y. conducted the ex vivo studies. J.W., H.Y., J.D., C.E.V., W.W., E.T.R., and C.F.G. designed the in vivo rat experiments. J.W., J.D., and H.Y. conducted the in vivo rat experiment. J.W. conducted in vitro cytotoxicity studies. L.G.G., T.L.S., C.S.N., J.D., and H.Y. designed and conducted the in vivo pig studies. J.D. conducted in vivo electrophysiological measurement and analysis. H.Y. and X.Z. developed the 3D-printing platform. J.D., H.Y., C.S.N., L.G.G., and X.Z. wrote the manuscript with input from all authors. **Competing interests:** J.D., H.Y., C.S.N, and X.Z. are inventors listed on a patent application that covers the bioadhesive pacing lead ("Bioadhesive pacing lead"; US Patent no. 63/562,123). H.Y., C.S.N., and X.Z. have a financial interest in SanaHeal. X.Z. has a financial interest in SonoLogi and Magnendo. The other authors declare that they have no competing interests. **Data and materials availability:** All data needed to evaluate the conclusions in the paper are present in the paper and/or the Supplementary Materials.

Submitted 26 February 2024
Accepted 29 May 2024
Published 19 June 2024
10.1126/scitranslmed.ado9003